



# 1 Seasonal Variability of the Oxygen Minimum Zone off Peru in a 2 high-resolution regional coupled model

3

4 O. Vergara<sup>1</sup>, B. Dewitte<sup>1</sup>, I. Montes<sup>2</sup>, V. Garçon<sup>1</sup>, M. Ramos<sup>3,4,5</sup>, A. Paulmier<sup>1</sup>, and O.  
5 Pizarro<sup>6</sup>

6

7 [1]{Laboratoire d'Études en Géophysique et Océanographie Spatiales, CNRS/CNES/UPS, UMR5566,  
8 Toulouse, France}

9 [2]{Instituto Geofísico del Perú (IGP), Lima, Perú}

10 [3]{Departamento de Biología, Facultad de Ciencias del Mar, Universidad Católica del Norte,  
11 Coquimbo, Chile}

12 [4]{Millennium Nucleus for Ecology and Sustainable Management of Oceanic Islands (ESMOI),  
13 Coquimbo, Chile}

14 [5]{Centro de Estudios Avanzado en Zonas Áridas (CEAZA), Coquimbo, Chile}

15 [6]{Departamento de Geofísica, Facultad de Ciencias Físicas y Matemáticas, Universidad de  
16 Concepción, Concepción, Chile}

17

18 Correspondence to: O. Vergara (oscar.vergara@legos.obs-mip.fr)



## 1 Abstract

2 In addition to being one of the most productive upwelling systems, the oceanic region off Peru is  
3 embedded in one of the most extensive Oxygen Minimum Zones (OMZs) of the world ocean. The  
4 dynamics of the OMZ off Peru remain uncertain, partly due to the scarcity of data and to the ubiquitous  
5 role of mesoscale activity on the circulation and biogeochemistry. Here we use a high-resolution  
6 coupled physical/biogeochemical model simulation to investigate the seasonal variability of the OMZ  
7 off Peru. The focus is on characterizing the seasonal cycle in Dissolved O<sub>2</sub> (DO) eddy flux at the OMZ  
8 boundaries, including the coastal domain, viewed here as the eastern boundary of the OMZ,  
9 considering that the mean DO eddy flux in these zones has a significant contribution to the total DO  
10 flux. Along the coast, despite the increased seasonal low DO water upwelling, the DO peaks  
11 homogeneously over the water column and within the Peru Undercurrent (PUC) in austral winter,  
12 which results from mixing associated with the increase in both the intraseasonal wind variability and  
13 baroclinic instability of the PUC. The coastal ocean acts therefore as a source of DO in austral winter  
14 for the OMZ core through eddy-induced offshore transport that is also shown to peak in Austral winter.  
15 In the open ocean, the OMZ can be divided vertically into two zones: an upper zone above 400m where  
16 DO eddy flux dominates over the mean seasonal DO flux, and varies seasonally, and a lower part  
17 where DO exhibits vertical-zonal propagating features and where the mean seasonal DO flux shares  
18 similar characteristics than those of the energy flux associated with the annual extra-tropical Rossby  
19 waves. At the OMZ meridional boundaries where the mean eddy flux is large, the DO eddy flux has  
20 also a marked seasonal cycle that peaks in austral winter (spring) at the northern (southern) boundary.  
21 In the model, the amplitude of the seasonal cycle is 67% larger at the southern boundary than at the  
22 northern boundary. Results implications for understanding the OMZ variability at longer timescales are  
23 discussed.



## 1 **1 Introduction**

2 In addition to hosting one of the most productive upwelling systems, the South Eastern Pacific (SEP) is  
 3 home to one of the most extensive Oxygen Minimum Zones (OMZs) of the world ocean (Fuenzalida et  
 4 al., 2009; Paulmier and Ruiz-Pino, 2009). These oxygen deficient regions are key to understand the  
 5 role of the ocean in the greenhouse gases budget and in climate, and in the present unbalanced nitrogen  
 6 cycle (Gruber, 2008). The OMZs represent a net nitrogen loss to the atmosphere in the form of N<sub>2</sub>O  
 7 (particularly the SEP OMZ: Farias et al., 2007; Arevalo-Martinez et al., 2015), in addition with other  
 8 toxic or climatic gases, such as H<sub>2</sub>S and CH<sub>4</sub>, respectively, in extremely low dissolved oxygen (DO)  
 9 concentrations (Libes, 1992; Law et al., 2013). They might even limit the CO<sub>2</sub> sequestration ocean role  
 10 and act as CO<sub>2</sub> sources for the atmosphere (Paulmier et al., 2008; 2011). Furthermore, the OMZs  
 11 represent a respiratory barrier for marine organisms, and restrain their niche habitat in a zone which  
 12 sustains 10% of the world fish catch (Chavez et al., 2008). Therefore, understanding the dynamics  
 13 behind the OMZ becomes not just a matter of scientific interest, but also a major societal concern.

14 In general, these low oxygen regions are considered to result from the interaction of biogeochemical  
 15 and physical processes (Karstensen et al., 2008). The SEP presents high biological productivity,  
 16 inducing a significant DO consumption mainly through the remineralization associated with a complex  
 17 nutrient cycle supported by the intense upwelling. In addition, the SEP encompasses a so-called  
 18 'shadow zone', a near stagnant/sluggish circulation region next to the eastern basin boundary, not  
 19 ventilated by the basin scale wind driven circulation (Luyten et al., 1983). Assuming a steady state,  
 20 lateral oxygen fluxes from subtropical water masses and diapycnal mixing are expected to balance the  
 21 oxygen consumption (Brandt et al., 2015). However, the diversity of environmental forcings in the SEP,  
 22 and the variety of timescales at which they operate (Pizarro et al., 2002; Dewitte et al., 2011; 2012) has  
 23 eluded a proper understanding of the processes controlling the OMZ structure and variability. On the  
 24 one hand, the scarcity of data and rare surveys have only permitted to document the DO temporal  
 25 variability at a few locations (e.g. Morales et al., 1999; Cornejo et al., 2006; Gutierrez et al., 2008;  
 26 Llanillo et al., 2013). On the other hand, the highly complex interaction between physical and  
 27 biogeochemical mechanisms makes modeling and prediction of OMZ location, intensity and its  
 28 temporal variability a challenging task (Karstensen et al., 2008; Cabré et al., 2015). Low resolution  
 29 CMIP class coupled models still have severe biases of physical and biogeochemical origins,  
 30 particularly in Eastern Boundary Current systems (Richter, 2015), which has eluded the interpretation



1 of long term trends in OMZ (Stramma et al., 2008; 2012; Cabré et al., 2015). Regional coupled  
2 biogeochemical modeling nonetheless has provided a complementary approach to gain insight in the  
3 dynamics of OMZ and its relationship with climate (Resplandy et al., 2012; Gutknecht et al., 2013a).  
4 One recent modeling effort in understanding the dynamics behind the OMZ in the Eastern Tropical  
5 Pacific comes from Montes et al. (2014). This study provided a first regional simulation of the OMZ in  
6 the SEP, and summarized the elements involved in maintaining the OMZ found off the coast of Peru as  
7 resulting from a delicate balance between (i) the equatorial current system dynamics: the relatively  
8 oxygen-rich waters carried by the Equatorial Undercurrent (EUC), the relatively oxygen poor and  
9 nutrient rich waters by the primary and secondary Tsuchiya Jets (primary and secondary Southern  
10 Subsurface Countercurrents, pSSCC and sSSCC, respectively), and (ii) the high surface productivity  
11 rates induced by the coastal upwelling, which in turn triggers an intense oxygen consumption in the  
12 subsurface. Their model experiments also showed that different Eddy Kinetic Energy (EKE) levels,  
13 induced by different representations of the mean vertical structure of the coastal current, may contribute  
14 to expand or erode the upper boundary of the OMZ.

15 The study by Montes et al. (2014) established a benchmark in terms of numerical modeling of the OMZ  
16 in the SEP, focusing on its permanent regime and connection with the equatorial current dynamics. In  
17 the present study, we also take advantage of the regional modeling approach in order to investigate the  
18 mechanisms associated with the seasonal cycle of DO within the OMZ. The motivation for focusing on  
19 seasonal variability is three-folds: 1) A better knowledge of the processes acting on the OMZ at  
20 seasonal timescale is viewed as a prerequisite for interpreting longer timescales of variability (ENSO,  
21 decadal); 2) the scarcity of quality long term subsurface biogeochemical data in the SEP is a limitation  
22 for tackling the investigation of OMZ variability at low frequency; 3) To the authors' knowledge, this  
23 issue has not been addressed in the literature for the Eastern Tropical Pacific, although it has been a  
24 concern for other tropical oceans (Resplandy et al., 2012; Gutknecht et al., 2013a; Duteil et al., 2014).

25 Here, besides investigating to which extent the seasonal OMZ variability can relate to the variability of  
26 the environmental forcing in the SEP (local wind, equatorial Kelvin and extra-tropical Rossby waves),  
27 our interest is on examining the DO budget (i.e. the balance between oxygen sources and sinks) and  
28 relating it to the physical DO flux. In particular, since the Peruvian region is the location of a relatively  
29 intense eddy activity (Chaigneau et al., 2009), the question of whether or not eddy activity is involved  
30 in the seasonal variability of the OMZ arises, and calls for assessing its contribution to the DO flux.





1 There is growing evidence that mesoscale activity has a key role on the biogeochemical cycles and the  
2 OMZ structure in EBUS (Duteil and Oschlies, 2011, Nagai et al., 2015). Most studies addressing the  
3 role of mesoscale processes in the OMZs have focused on the ventilation from the coastal domain,  
4 where the primary production bloom provides nutrients and DO anomalies that are in turn transported  
5 offshore (Stramma et al., 2013; Czeschel et al., 2015). Gruber et al. (2011) showed that mesoscale  
6 activity is prone to reduce the biological production and offshore export in upwelling systems by both  
7 rectifying on the mean circulation (i.e. eddies-induced mixing tends to flatten the isotherms nearshore  
8 and reduce the upwelling) and changing its nutrient transport capacity. This process has been to some  
9 extent supported by observations in the Peruvian OMZ (Stramma et al., 2013). In this sense, the  
10 mesoscale activity represents a ventilation pathway for the OMZ, through the offshore transport of  
11 OMZ properties. The ventilation of the OMZ could also take place at its meridional boundaries where  
12 strong mean DO gradients are found along with eddy activity. Recently, Bettencourt et al. (2015)  
13 proposed that mesoscale eddies shape the Peruvian OMZ by controlling the diffusion of DO into the  
14 OMZ at the meridional boundaries. Although it is likely that both processes are important for  
15 understanding the OMZ structure, it has not been clear to which extent the variability of the OMZ  
16 could be understood in terms of the changes in the eddy DO flux into the OMZ through these different  
17 pathways. The mesoscale activity also exhibits a significant meridional variability off Peru (Chaigneau  
18 et al., 2009), which questions if the offshore ventilation process can operate effectively for modulating  
19 the whole OMZ. Another related open question is at which timescales the ventilation process through  
20 eddies-induced mixing can operate effectively. In this paper we will tackle these issues from a regional  
21 modeling approach, focusing on the seasonal timescale.

22 The paper is organized as follows. After the Introduction (Section 1), we detail the observations and  
23 model configuration used in the study, as well as the methodology employed in the treatment of the  
24 information (Section 2). We also evaluate the realism of the simulation against the available  
25 observations in reproducing the main characteristics of the OMZ. The subsequent section (Section 3)  
26 characterizes the DO annual cycle inside the OMZ. Section 4 opens with the analysis of the seasonal  
27 variability of the coastal OMZ, and the contribution of the DO budget terms associated with it. This  
28 analysis is followed by the results on DO flux directed offshore and completed by the analysis of DO  
29 flux across the OMZ meridional boundaries. The final section (Section 5) presents a summary and a  
30 discussion of the main results, followed by perspectives for future work.



1

## 2 **2 Data description and Methods**

### 3 **2.1 Data**

#### 4 **Dissolved Oxygen concentration from CARS**

5 The CSIRO Atlas of Regional Seas (CARS) is a climatological product derived from a quality-  
 6 controlled archive of historical subsurface ocean measurements, most of which was collected during  
 7 the past 50 years (Additional information might be found in the website of the project:  
 8 <http://www.marine.csiro.au/~dunn/cars2009/>). For the present study, we use the CARS2009 version of  
 9 the CARS product (Ridgway et al., 2002), which has an horizontal resolution of  $0.5^\circ \times 0.5^\circ$  and 79  
 10 vertical levels, with a 10m resolution near the surface layer. We use CARS to assess the model skills in  
 11 simulating the OMZ mean state and variability. One advantage of this product is its refined  
 12 interpolation treatment near steep topography, in comparison to other products such as the World  
 13 Ocean Atlas (Dunn and Ridgway, 2002). Also, it includes the annual and semiannual oxygen cycles,  
 14 although the semiannual cycle is available only for the first 375 m over the region of interest due to the  
 15 scarcity of data.

#### 16 **Chlorophyll-a concentration from SeaWiFS**

17 SeaWiFS 8 day composites at  $0.5^\circ \times 0.5^\circ$  resolution chlorophyll product (version 4), between January  
 18 2000 and December 2008, is used to compute the surface chlorophyll seasonal cycle at  $12^\circ\text{S}$  (McClain  
 19 et al., 1998; O'Reilly et al., 2000).

### 20 **2.2 Model simulation**

21 We use a high resolution simulation of the South Eastern Pacific, based on the hydrodynamic model  
 22 Regional Ocean Modeling System (ROMS) circulation model (see Shchepetkin and McWilliams,  
 23 2005; 2009 for a complete description of the model) coupled with a nitrogen-based biogeochemical  
 24 model developed for the Eastern Boundary Upwelling Systems (BioEBUS, Gutknecht et al., 2013ab),  
 25 hereby referred as CR BIO.

26 The model is used at an eddy-resolving resolution ( $1/12^\circ$  at the equator) for a region extending from  
 27  $12^\circ\text{N}$  to  $40^\circ\text{S}$  and from the coast to  $95^\circ\text{W}$  -nevertheless this study only focuses on the domain spanning  
 28 the latitudes of Peru and Ecuador (Fig. 1)- with lateral open boundaries at its northern, southern and  
 29 western frontiers. The physical model resolves the hydrostatic primitive equations with a free-surface  
 30 explicit scheme, and a stretched terrain-following sigma coordinates on 37 vertical levels. The



1 configuration is similar to Dewitte et al. (2012), that is the open boundary conditions are provided by  
2 3-daily mean oceanic outputs from SODA (Version 2.1.6) for temperature, salinity, horizontal velocity  
3 and sea level for the period 1958-2008, while wind stress and speed forcing at the air/sea interface  
4 come from the NCEP/NCAR reanalysis. The atmospheric fields have been statistically downscaled  
5 following the method by Goubanova et al. (2011) in order to correct for the unrealistic wind stress curl  
6 near the coast of the NCEP Reanalysis (see Cambon et al. (2013) for a validation of the method for  
7 oceanic applications). Atmospheric fluxes were derived from the bulk formula using the temperature  
8 from COADS 1°x1° monthly climatology (daSilva et al., 1994). Relative humidity and short wave and  
9 long wave radiations are also from COADS. Bottom topography is from the GEBCO 30 arc-second  
10 grid data set, interpolated to the model grid and smoothed as in Penven et al. (2005) in order to  
11 minimize the pressure gradient errors and modified at the boundaries to match the SODA bottom  
12 topography. This model configuration has been validated from observations and has exhibited good  
13 skills in simulating the mean circulation off Peru and its interannual variability (see Dewitte et al.  
14 (2012)).

15 The ocean model within this configuration is coupled to the BioEBUS model following similar  
16 methodology than Montes et al. (2014). BioEBUS uses two compartments of phytoplankton and  
17 zooplankton, small (flagellates and ciliates, respectively) and large (diatoms and copepods,  
18 respectively), detritus, dissolved organic nitrogen and the inorganic nitrogen forms nitrate, nitrite and  
19 ammonium, as well as nitrous oxide (see Gutknecht et al., 2013ab, for a description of the model). The  
20 open-boundary conditions for the biogeochemical model are provided by the climatological CARS data  
21 set (nitrate and oxygen concentrations) and by SeaWiFS archive (chlorophyll-a concentration).  
22 Additional biogeochemical tracers are computed following Gutknecht et al. (2013ab). Initial  
23 phytoplankton concentration is defined as a function of vertically extrapolated satellite Chl-a following  
24 Morel and Berthon (1989). An offshore decreasing cross shore profile, following in situ observations, is  
25 applied for zooplankton, and a vertical constant (exponential) profile is used for detritus (nitrite,  
26 ammonium and dissolved organic nitrogen), respectively. In order to get a realistic solution for the  
27 region, the model parameters were tuned to simultaneously fit modeled oxygen and nitrate fields to  
28 observations (see Table A1 of Montes et al. (2014) for parameter values). These changes were  
29 motivated by the need to adjust the microbiological rates to values observed in the SEP. Within this  
30 parameter configuration, BioEBUS has been shown to be skillful for simulating the OMZ off Peru



(Montes et al., 2014). In particular the pattern correlations between the model and observations for both the annual mean and the seasonal cycle inside the OMZ present comparable scores ( $>0.85$ , cf. Montes et al. (2014)) as well as low standard deviations (i.e. in the order of the observed values). We focus on the last 10 years of the simulation which insures that the OMZ equilibrium is reached. The year 1958 has been repeated 10 times so that the actual spin up consists in 53 years. The reason for focusing on the last ten years of our simulation is also motivated by the fact that the atmospheric momentum forcing is close to the satellite QuickSCAT winds by construction (see Goubanova et al. (2011) for details) so that this period of the simulation is the one when the model is the most constrained by observations. A monthly mean climatology is calculated for all variables over this period from the 3-day mean outputs of the model, which can be compared to the CARS data. Consistently with Montes et al. (2014), the coupled simulation is skillful in simulating the mean characteristics of the OMZ off the Peruvian coast (Figures 1 and 2). In particular the thickness and location of the model OMZ core limits are realistic, and in good agreement with previous studies (Fig. 1; e.g. Paulmier et al., 2006; Cornejo and Farias, 2012; Montes et al. 2014). Close to the western boundary of our model domain, the simulated OMZ also exhibits a realistic vertical structure (Fig. 2) with comparable concentration in DO than observations in the vicinity of the Equatorial Undercurrent ( $\sim 100$  m; Equator). Furthermore, the simulation is consistent in reproducing the oxygen consuming processes, as supported by the Apparent Oxygen Utilization (AOU; Fig. 3), also in good agreement with previous studies (cf. Figure 8 in Cabré et al. (2015)). AOU was computed as the difference between the DO concentration and the saturated oxygen ( $O_2\text{sat}$ ) concentration ( $\text{AOU} = O_2\text{sat} - O_2$ ) with  $O_2\text{sat}$  following the methodology of Garcia and Gordon (1992). The realistic representation of the oxygen consuming processes is reflected by the Particulate Organic Carbon flux as well (Fig. 4a), whose values at 100m fall within the observed range for the region ( $30\text{--}60 \text{ gC m}^{-2} \text{ yr}^{-1}$  in the shelf area; Dunne et al., 2005; Henson et al., 2012). In addition, the low transfer efficiency of carbon (10–15% or lower over and next to the shelf; Henson et al., 2012), from the euphotic zone to greater depths (Fig. 4b), implies that the remineralization processes take place at realistic depths, and therefore allow for a correct vertical representation of the OMZ (cf. Fig. S2 in Cabré et al. (2015) for comparison). The core of the OMZ, defined with a suboxic concentration ( $[\text{DO}] < 20 \mu\text{M}$ ;  $\mu\text{M}$  will be used to refer to  $\mu\text{mol L}^{-1}$  in all the text and figures), occupies nearly 23% of the domain volume (Fig. 5a), with the less oxygenated layers comprised between  $5^\circ\text{S}$  and  $15^\circ\text{S}$ , and 100 m and 600 m depth (Fig. 2). As expected,



1 the simulation presents a finer spatial variability than the climatological product (Fig. 2). Moreover, we  
 2 computed a geographical OMZ overlapping metric following Cabré et al. (2015), which quantifies the  
 3 spatial agreement of the OMZ volume distribution between the simulation and CARS, varying between  
 4 0 (no agreement) and 1 (perfect collocation). We obtained a value of 0.79, which is ~58% above the  
 5 best CMIP5 models used in Cabré et al. (2015).  
 6 Despite the overall good agreement between the model and observations, the modeled oxygen content  
 7 is however underestimated as compared to CARS in certain regions of the domain, particularly  
 8 southwards of 20°S (Fig. 2a) and close to the coast (Fig. 2b). The modeled DO distribution is also  
 9 characterized by finer spatial scales of variability inside the OMZ compared to observations (Figures  
 10 2c and 2d). In particular, the model oxycline is shallower and with a more intense DO gradient than the  
 11 observations, which has been also observed in a simulation of the Arabian Sea OMZ (Resplandy et al.,  
 12 2012), suggesting that the CARS data set may not have a sufficient vertical resolution to realistically  
 13 resolve the oxycline at some locations. Also, it must be kept in mind that CARS is built using all the  
 14 available data from the second half of the twentieth century (1940-2009), whereas we focus on the  
 15 period 2000-2008 for the simulation, which is known to be a colder period than the previous decades in  
 16 the eastern tropical Pacific (Henley et al., 2015). Other limitation for the comparison between model  
 17 and data includes the errors associated with the scarcity of data in some regions (Bianchi et al., 2012).  
 18 Nonetheless, the simulation is in good agreement with CARS in terms of mean characteristics of the  
 19 OMZ, as well as the mean oxygen concentration and its distribution (Figures 3, 5a).  
 20 In order to evaluate the realism of the seasonal cycle, we estimate the seasonal variability of the  
 21 volume of water within the suboxic DO concentration range 0-20  $\mu\text{M}$  in both the model and data (Fig.  
 22 5b). The results indicate that, despite a weaker amplitude (by 15% on average), the seasonal cycle of  
 23 the OMZ core is relatively well simulated by the model. For hypoxic DO volume in the range 40-50  
 24  $\mu\text{M}$ , the agreement is as good as inside the OMZ core, with a Pearson correlation value of 0.9 and a  
 25 volume RMS difference of 16%, between the simulation and the observations. The good agreement of  
 26 the seasonal cycle between CARS and the simulation, in addition to the consistency of our results with  
 27 those of Montes et al. (2014), provides confidence in using the model outputs for investigating the  
 28 processes associated with the seasonal variability of the OMZ.

## 29 **2.3 Methods**



1 In this work, our approach is twofold: First, the biogeochemical processes for DO are investigated  
 2 explicitly through the on-line oxygen budget (1). Although this methodology can provide a direct  
 3 estimate of the seasonal variability in advection and mixing, it does not allow for a direct estimate of  
 4 the eddy contribution to DO change that can also vary seasonally. The DO flux associated with  
 5 different timescales of variability is therefore estimated. The latter consists in calculating the temporal  
 6 average of the cross-products between DO and velocity anomalies. Anomalies can refer either to  
 7 seasonal anomalies and in that case, this provides the seasonal DO flux, or to the intraseasonal  
 8 anomalies (calculated here as the departure from the monthly mean) and in that case, this provides an  
 9 estimate of the DO eddy flux. We also estimated the seasonal activity of the DO eddy flux, which  
 10 consists in calculating the DO eddy flux over a 3-month running window and then a monthly  
 11 climatology of this quantity. The climatological EKE activity is estimated similarly.

12 The DO budget consists in the following Equation:

$$13 \quad \frac{\partial O_2}{\partial t} = -\mathbf{u} \cdot (\nabla O_2) + K_h \nabla^2 O_2 + \frac{\partial}{\partial z} \left( K_z \frac{\partial O_2}{\partial z} \right) + SMS(O_2). \quad (1)$$

14 The first three terms on the right hand side represent the physical processes involved in the changes in  
 15 oxygen concentration. The first term stands for the advection of oxygen (with  $\mathbf{u}$  the velocity vector),  
 16 the second term corresponds to the horizontal diffusion (with  $K_h$  the eddy diffusion coefficient), and the  
 17 third term corresponds to the vertical mixing (with turbulent diffusion coefficient  $K_z$ ). The fourth term  
 18 represents the “Sources-Minus-Sinks” contribution to the oxygen changes, directly due to  
 19 biogeochemical activity. Biogeochemical processes correspond to the sum of oxygen sources and sinks,  
 20 namely the photosynthetic production, and the aerobic processes (oxic decomposition, excretion and  
 21 nitrification). In this study, for simplicity, those will be considered as a summed-up contribution to the  
 22 DO rate of change, whereas physical processes will be divided into advection and mixing terms. Each  
 23 term of this oxygen budget is determined on line at each time integration.

24 In the SEP, the subthermocline seasonal variability can be interpreted as resulting from the propagation  
 25 of Extra-Tropical Rossby Waves (ETRW). ET RW radiate from the coast and propagate vertically,  
 26 inducing a vertical energy flux, whose trajectory follows the theoretical Wentzel-Kramers-Brillouin  
 27 (WKB) ray paths (Dewitte et al., 2008; Ramos et al., 2008). The energy flux results from the phase  
 28 relationship between vertical velocity associated with the vertical displacement of the isotherms, and  
 29 the pressure fluctuations associated with them. In the regions sufficiently below the thermocline for



DO consumption to become weak (that is DO can be considered a passive tracer), it is expected that changes in DO relate to the anomalous velocity field, and that the DO flux shares comparable characteristics than the Eliassen-Palm flux (EP flux; Eliassen and Palm, 1960). In order to derive the trajectories of the WKB ray paths, a vertical mode decomposition of the mean model stratification at each grid point of the simulation was performed, which provides the phase speed values of each baroclinic mode. According to the theory, in the case of vertical/westward propagation, the highest amplitudes should be found along the WKB trajectories, and the phase lines should orientate approximately parallel to the WKB ray paths. For details on the WKB theory applied to the extra tropical latitudes, the reader is invited to refer to Ramos et al. (2008).

10

### 11 **3 Characteristics of the DO annual cycle**

As previously stated, the annual signal is a conspicuous feature inside the region (Fig. 5), although it manifests differently across the OMZ. As an illustration, the amplitude and phase of the annual harmonic of the model DO climatology is presented along a section off central Peru (12°S, Fig. 6ab), where the OMZ core is extensive (Fig. 1). The DO climatology has been normalized by its RMS (Root Mean Square), in order to emphasize the regions where the amplitude in DO changes (and mean DO) is weak. The amplitude reveals a complex pattern with three regions of large relative variability: 1) near the coast (i.e. fringe of ~150 km) between the oxycline and 400 m; 2) offshore between 82°W and 84°W in the upper 400 m and 3) below 500 m. The phase lines over these three regions suggest distinct propagating characteristics: whereas in the coastal region there is no propagation, in the offshore and deep region, there is indication of a westward propagation. In the region below 500 m, the phase lines tend also to be parallel and slope downward, suggestive of westward-downward propagation (estimated phase speed of ~2.5 cm s<sup>-1</sup>). These propagating characteristics can be evidenced in the Hovmöllers of the recomposed annual cycle at the depth of 150 m (Fig. 6c) and 700 m (Fig. 6d). While at 150 m the annual signal does not clearly propagate and only shows two domains of high amplitude, separated by low amplitude values (Fig. 6c), there is a clear westward propagation of the DO anomalies at 700 m, with the phase speed increasing westward. At 400 m, the propagation is only observed west of 81°W (Fig. 6b). In addition to the large vertical structure variability of the annual cycle, the OMZ annual cycle is also characterized by a large horizontal variability in particular at its northern and southern boundaries. This is illustrated from Figure 7, that displays the amplitude of the annual cycle of the DO





1 climatology at 400 m, and evidences amplitude peaks at the OMZ meridional boundaries (between the  
 2 20 and 45  $\mu\text{M}$  isopleths).

3 The annual variability pattern evidenced above results from a delicate balance between the physical  
 4 processes (namely advection and mixing) and the biogeochemical processes (consumption versus  
 5 production). As a first step towards investigating each term of the DO budget, it is interesting to  
 6 evaluate the relative contribution of the physical and biogeochemical fluxes to the DO variability at  
 7 seasonal scale. The RMS of the climatological fluxes along a section at 12°S indicates that the  
 8 maximum amplitude of the seasonal fluxes takes place near the oxycline and along the coast over the  
 9 whole water column (Figure 8). The relative importance of the physical processes against the  
 10 biogeochemical processes varies across the OMZ. At the coast and near the oxycline, the annual  
 11 variability of the biogeochemical processes reaches values almost half those of the variability in  
 12 physical processes (Fig. 8c), as a consequence of the proximity to both the well lit and highly  
 13 productive part of the water column, and the high remineralization activity that occurs near the  
 14 oxycline. Towards offshore and at depth, the relative importance of the variability of the  
 15 biogeochemical processes reduces gradually. Near ~300 m the variability of the biogeochemical  
 16 processes is nearly 1/5 of the physical processes variability. Below ~300 m, and towards the lower part  
 17 of the OMZ core and below, the physical processes variability is one order of magnitude larger.  
 18 Consequently, the distribution of DO in the lower part of the OMZ is rather a function of  
 19 advection/diffusion than a consequence of the biogeochemical processes, although DO consumption  
 20 even at very low levels has the potential to generate local gradients and therefore induce advection. The  
 21 spatial heterogeneity in the seasonal DO changes induced by the biogeochemistry and dynamics as  
 22 described above, appears as an ubiquitous feature in the OMZ. To illustrate this, we estimate the  
 23 proportion of explained variance of the seasonal DO rate of change by the physical fluxes as:

$$24 \quad R^2_{\text{Phys.}} = \left(1 - \frac{\text{RMS}(\text{Biogeochemical Fluxes})}{\text{RMS}(\text{Total Fluxes})}\right) \cdot 100 . \quad (2)$$

25 Figure 9ab presents the results of  $R^2_{\text{Phys.}}$  at 100 and 450 m depth, which evidences that the relative  
 26 importance of the physical fluxes versus the biogeochemical fluxes in the seasonal DO variability  
 27 increases with depth, and is enhanced at the OMZ boundaries. On the other hand, the biogeochemical  
 28 fluxes explain more than 50% of the variance in seasonal DO change rate in a narrow (~ 200 km width)  
 29 coastal fringe that extends more offshore to the north of the domain (around 8°S; Fig. 9a) and vertically





1 down to 300 m (Fig. 9c).  
 2 Based on the above analysis, it is clear that the coastal region (first 200-300 km from the coast) below  
 3 the oxycline corresponds to a territory where the seasonal variability of biogeochemical and physical  
 4 fluxes have a comparable magnitude, whereas outside this region, notably in the lower part of the OMZ  
 5 core, the physical fluxes variability dominates over the biogeochemical fluxes variability at seasonal  
 6 timescale. Hereafter we examine the possibility of two distinct regimes of OMZ dynamics at seasonal  
 7 timescale: one associated with the upper OMZ (including coastal domain and meridional boundaries),  
 8 and the other one associated with the deep OMZ. In the following we investigate the processes  
 9 responsible for the DO flux.

10

#### 11 **4 Seasonality of the OMZ ventilation**

12 It has been shown for the SEP that the DO content near the coast is set to a large extent from the  
 13 transport of oxygen deficient waters from the equatorial current system, particularly the oxygen  
 14 depleted sSSCC (Montes et al., 2014). Therefore, the seasonal variability of DO is likely to result in  
 15 part from the seasonal variability of the different branches of the EUC in the far eastern Pacific. Local  
 16 wind stress forcing (and its intraseasonal activity) has also a marked seasonal cycle off Peru (Dewitte et  
 17 al., 2011) which may impact both the upwelling dynamics -through Ekman pumping/transport- and  
 18 mixing. Some studies also argue that the ventilation of the OMZ takes place through the offshore  
 19 transport of oxygen (deoxygenated) by eddies from the coastal domain (Czeschel et al., 2011),  
 20 implying that the variability of such processes is set up by coastal processes that determine the nature  
 21 of the DO source. As a first step, we investigate the mechanisms responsible for the seasonal variability  
 22 in DO along the coast, which can be considered as the eastern boundary of the OMZ. This is aimed at  
 23 providing material for the interpretation of the offshore DO flux variability.

##### 24 **4.1 The coastal domain as the eastern boundary of the OMZ: variability and** 25 **mechanisms**

26 Figure 10 displays the dominant EOF mode of various climatological fields in a section at 12°S near  
 27 the coast and from the oxycline (45  $\mu M$  isoline) to the depth of 300 m. Figure 11 shows the principal  
 28 components associated with these dominant EOF mode patterns. The seasonal DO cycle is dominated  
 29 by an annual component, with a peak centered in August (Fig. 11a), and the largest variability at the  
 30 coast below the oxycline that extends offshore and downward, resulting in an elongated tongue below



1 100 m near  $\sim 78^{\circ}\text{W}$  (Fig. 10a). During the first quarter of the year, oxygen anomalies remain relatively  
2 stable (oxygen rate nearly zero, Fig. 11b), and negative, due to a high production of organic matter in  
3 Austral summer (cf. Fig. 1c of Gutierrez et al., 2011) that stimulates a subsurface oxygen consumption  
4 associated with the degradation of this organic matter. DO anomalies start to increase during the second  
5 quarter, become positive in June and reach their maximum in August (Fig. 11a). The peak anomaly in  
6 Austral winter could be understood in terms of the increased mixing (see Fig. 11a showing EKE  
7 peaking in July) associated with the increase in baroclinic instability due to the seasonal intensification  
8 of the PUC from June. Note that the pattern of the dominant EOF of the alongshore current coincides  
9 with the mean position of the PUC (see Fig 10b), so that seasonal variations of the PUC can be  
10 interpreted in terms of the variations in the vertical shear of the coastal current system. Other processes  
11 that may explain the peak DO anomaly in Austral winter includes the reduced productivity and  
12 downwelling that peaks in June (Fig. 11c), associated with seasonal equatorial downwelling Kelvin  
13 wave.

14 The following investigates the tendency terms of the DO budget, in order to quantitatively interpret the  
15 DO seasonal cycle near the coast. Given that the analysis is performed inside the  $45\ \mu\text{M}$  isopleth, the  
16 biogeochemical flux term is largely dominated by the “Sinks” terms (aerobic processes; one order of  
17 magnitude larger than “Sources”), driven by organic matter remineralization and zooplankton  
18 respiratory metabolic terms (not shown). For clarity, the seasonal DO budget is presented synthetically,  
19 from the dominant EOF mode of the climatological advection, mixing and biogeochemical fluxes  
20 terms. Although this does not warranty a perfect closure, it eases the interpretation. Note that the  
21 residual resulting from the difference between the first EOF mode of the rate of DO changes and all the  
22 other terms in Figure 11b is rather weak, validating to some extent our approach. First of all, we find  
23 that the largest amplitude of the mode patterns is found near the coast and inside the mean PUC core  
24 (Figs. 10d to 10g). During the first part of the year (January to May), positive and constant advection  
25 anomalies are compensated by mixing, and maintain the rate of DO change close to zero (Fig. 11b).  
26 Biogeochemical fluxes anomalies are positive during that period, associated with a positive anomaly of  
27 primary production in the well lit surface layers, implied by the high chlorophyll-a values (Fig .11c). A  
28 positive oxygen anomaly is sustained by the advection terms and the biogeochemical terms, and is  
29 balanced out by the constant input of low oxygen waters carried by the PUC (Montes et al. 2010;  
30 2014), generating the relatively stable oxygen values (oxygen rate nearly zero).



1 From May, the rate of DO changes increases concomitantly with EKE (Fig. 11ab), followed one month  
2 later by mixing, whereas advection and biogeochemical fluxes decrease. By June-July, the  
3 intensification in alongshore winds (Fig. 11c) starts to propel the coastal upwelling, which has two  
4 compensating effects: on one hand it triggers photosynthesis in the lit surface layers (DO rate turns to  
5 positive values) and on the other, it uplifts low oxygen waters from the OMZ. The intraseasonal wind  
6 activity also starts to increase at that time (cf. Fig. 11c; see also Dewitte et al., 2011) which favors  
7 mixing, and so the downward intrusion of positive DO anomalies (note the deepening of the mixed  
8 layer in Fig. 11c). The overall effect is an increase in DO which leads to a peak anomaly in August. At  
9 that time, the DO rate drops sharply due to the strong subsurface DO consumption associated with  
10 aerobic remineralization of organic matter produced earlier in the season (DO rate moves sharply to  
11 negative values) and the high mixing that brings DO depleted waters from the subsurface into the  
12 deepened mixed layer. Note that this is consistent with the decrease in surface chlorophyll-a (Fig. 11c)  
13 and the interpretation proposed by Echevin et al. (2008) to explain the Austral summer minimum in  
14 surface chlorophyll-a observed off Central Peru.

15 This change to oxygen poor conditions combines with the natural decrease in oxygen production  
16 towards the end of the upwelling season and coincides with a restratification of the water column,  
17 which restricts the oxygenated waters near the surface (Echevin et al., 2008). This altogether  
18 contributes to maintain a negative DO rate inside the coastal OMZ, despite the increase in anomalous  
19 DO flux from the advective terms and (later on) biogeochemical processes towards the end of the year.  
20 As a result, oxygen returns to low values towards the end of the year.

## 21 **4.2 Offshore flux**

22 While the coastal OMZ variability is heavily constrained by the environmental forcings –coastal  
23 upwelling, coastal current system and local wind– due to the shallow oxycline there, the offshore  
24 OMZ, as embedded in the shadow zone of the thermohaline circulation, is somewhat insensitive to  
25 direct local forcing and rather experiences remote influence in the form of westward propagating  
26 mesoscale eddies (Chaigneau et al., 2009) and ETRW (Ramos et al., 2008; Dewitte et al., 2008). The  
27 influence of westward propagating mesoscale eddies on the OMZ translates as the transfer of coastal  
28 water properties towards the open ocean (DO included), while these properties are altered during  
29 transport due to physical-biogeochemical interactions (Stramma et al., 2014; Karstensen et al., 2015).  
30 Towards the end of their lifetime, hydrographic and biogeochemical anomalies carried by eddies are



1 redistributed in the ocean (Brandt et al., 2015), linking the coast and the open ocean. Although most  
 2 eddies genesis takes place near the coast (Chaigneau et al., 2009) and seasonal ETRW have a coastally  
 3 forced component (Dewitte et al., 2008), we expect different characteristics of the seasonal variability  
 4 in DO between the coast and the open ocean, given that oxygen demand will change from one region to  
 5 the other. We also distinguish the mean DO flux associated with the annual component of the  
 6 circulation that represents the transport in DO associated with seasonal change in the large scale  
 7 circulation, and the annual variability of the eddy DO flux that corresponds to the annual changes in the  
 8 transport due to eddies. These two quantities are diagnosed at 12°S (results presented in Figs. 12ac).  
 9 The DO has been normalized by its climatological variability in order to emphasize variability patterns  
 10 where DO is low.

### 11 **Mean seasonal flux**

12 We now document the mean DO flux associated to the annual component of the circulation. Relatively  
 13 to the DO seasonal variability, the amplitude of the seasonal DO flux is maximum near the coast and  
 14 below ~400 m and it tends to be orientated westward-downward, following approximately the  
 15 trajectories of theoretical WKB paths for the annual period Rossby wave (Fig. 12a). Note that this is  
 16 consistent with the westward propagating pattern of DO below 400 m evidenced earlier (Fig. 6). As a  
 17 consistency check, we also estimated the annual energy flux vector in the (x,z) plan associated to a long  
 18 extra tropical Rossby wave, that is ( $\langle p^{1yr} u^{1yr} \rangle$ ,  $\langle p^{1yr} w^{1yr} \rangle$ ) where the superscript denotes the annual  
 19 harmonics and the bracket the temporal average (Fig. 12b). The flux vector indicates vertical  
 20 propagation of energy at the annual period and the pattern of maximum flux coincides approximately  
 21 with the region of maximum amplitude of the mean seasonal DO flux. This suggests that the annual  
 22 ETRW is influential on the DO flux below ~400 m. This is interpreted as resulting from the advection  
 23 of DO by the ETRW since biogeochemical fluxes have much less influence on the DO rate of change  
 24 below 400 m (Fig. 8c) and the amplitude of the annual cycle of climatological eddy DO flux has a  
 25 much reduced amplitude below that depth (Fig. 12c) suggesting a reduced contribution of mixing to the  
 26 DO budget. Note that the DO (Fig. 12c) was normalized prior to compute the oxygen eddy flux in  
 27 order to render both the analysis akin, and therefore contrast the flux associated with ETRW against the  
 28 annual oxygen eddy flux. It was verified that the vertical structure variability of the annual DO flux  
 29 described above for the section of 12°S is comparable at other latitudes within the OMZ. In particular  
 30 the annual DO flux tends to remain homogeneous along trajectories mimicking the energy paths of the



1 ETRW at annual period which slope becomes steeper to the South (not shown).

## 2 **Seasonal eddy flux**

3 The annual amplitude of the climatological DO eddy flux is thus the largest in the upper 400 m near the  
 4 coast at 12°S consistently with the high EKE in this region. Since EKE is large along the coast of Peru,  
 5 an offshore transport of DO by eddies is expected at all latitudes. Figure 13 presents the annual  
 6 harmonic of the climatological eddy DO flux along the coast and averaged in a coastal fringe distant 1°  
 7 from the coast and 2° width. The maximum amplitude –reaching  $\sim 1 \text{ cm s}^{-1} \mu\text{M}$ – is concentrated in the  
 8 upper oxycline (Fig. 13a) with a peak during Austral winter. The peak season is also confirmed by the  
 9 EOF analysis of the climatological eddy DO flux (not shown). Despite the relative large meridional  
 10 variability in the amplitude, the mean vertical structure of the eddy flux consists in an approximate  
 11 exponentially decaying profile with depth with a typical decay scale of  $\sim 90 \text{ m}$  (Fig. 13b) so that at 300  
 12 m the seasonal eddy flux is only 19% of that at 100 m on average along the coast. Figure 13a also  
 13 reveals that the annual eddy DO flux is larger towards the northern rim of the domain and extends  
 14 deeper than towards the south. The high values are increasingly confined close to the surface towards  
 15 the southern part of the domain in comparison to the northern part, although the vertical attenuation  
 16 displays a similar scale.

## 17 **4.3 Meridional boundaries**

18 Here, our objective is to document the seasonality of the eddy DO flux, considering the marked  
 19 seasonal cycle in EKE and oxygen eddy flux observed in this region. As a first step, we estimate the  
 20 distribution of mean eddy flux, in order to identify the regions where its magnitude is large and thus  
 21 where it is likely to vary seasonally with a significant amplitude.

## 22 **Mean seasonal flux**

23 The horizontal distribution of mean oxygen eddy flux displays the highest values at the boundaries of  
 24 the OMZ core (Fig. 14), and adjacent to the  $45 \mu\text{M}$  isopleth. Towards the inner OMZ, the mean oxygen  
 25 eddy flux values decrease notoriously, with a factor of nearly 10 between the interior and exterior of  
 26 the  $10 \mu\text{M}$  contour. In agreement with the observations reported in the previous section, the mean  
 27 oxygen eddy flux decreases sharply with depth (approximately one order of magnitude between 100 m  
 28 and 700 m), with the highest values concentrated near the oxycline as expected from the increasing  
 29 oxygen concentration in this part of the OMZ. In this sense, the pattern of oxygen eddy flux around the  
 30 depth of the oxycline encloses a region of high variability (not shown).



1 To gain further insight with respect to the vertical structure of the oxygen eddy flux and at the same  
 2 time, diagnose the role of the mesoscale activity at the boundaries of the OMZ, we compute the mean  
 3 oxygen eddy flux across the two sections (depicted in Fig. 14), which fairly agree with the OMZ  
 4 northern and southern limits (Fig. 15) and correspond to the provinces of high amplitude previously  
 5 identified (Fig. 13). The oxygen eddy flux across each of the north and south boundaries was computed  
 6 by averaging the product of the fluctuating velocity component normal to the boundary in the  
 7 horizontal directions and the fluctuating DO concentration component, thereby obtaining horizontal  
 8 eddy fluxes.

9 As observed in Figure 14, the highest values for both north and south boundary sections are also  
 10 comprised between the oxycline and the lower OMZ core limit, being almost one order of magnitude  
 11 smaller at greater depths (Fig. 15c). These high values, located between ~100-300 m, are followed by a  
 12 sharp decrease (average decrease of  $1.5 \text{ cm s}^{-1} \mu\text{M}$  in 100 m). At the range of depths between 100 m  
 13 and 300 m, the DO eddy flux displays higher values at the southern boundary (nearly twice as large)  
 14 when compared with the northern boundary. This ratio tends to vanish when analyzing the lower part of  
 15 the OMZ. At both boundaries, there is a gap of nearly one order of magnitude in the difference between  
 16 the lower and upper parts of the OMZ.

### 17 **Seasonal eddy flux**

18 We now document the seasonal variability of the oxygen eddy flux across the OMZ boundaries  
 19 analyzed above (Fig. 15). An EOF analysis of the mean seasonal cycle of the oxygen eddy flux is  
 20 performed at the boundary sections previously defined. The figure 16 presents the dominant EOF mode  
 21 patterns along with the associated timeseries. In order to estimate the uncertainty associated with the  
 22 location of the OMZ boundaries, we repeated this analysis for 12 nearby sections parallel to the  
 23 boundaries and spaced by  $0.2^\circ$ . This leads to an estimated dispersion (standard deviation across the  
 24 different sections) of the oxygen eddy flux. The dispersion is represented as a colored shading in the  
 25 Figures 16bde. At both locations, the first EOF accounts for a well defined seasonal cycle. At the  
 26 northern boundary (Fig. 16a), the seasonal cycle of the DO eddy flux peaks in Austral Winter, in phase  
 27 with the DO changes along the coast (Fig. 13). Note that the seasonal cycle is in phase with the one of  
 28 the intraseasonal activity of the horizontal current normal to the section, which was estimated the same  
 29 way than the climatological eddy flux (see red line in Fig. 16b), supporting the idea that the  
 30 climatological DO eddy flux results from anomalous advection. The amplitude of the mode pattern is



1 maximum at the oxycline with DO between 20 and 45  $\mu\text{M}$ , and presents a sharp decrease below the  
 2 OMZ core depth (Fig. 16a). This sharp decrease is evidenced by the mean vertical profile of the eddy  
 3 flux seasonal variability estimated as the RMS across the section of the EOF mode pattern (Fig. 16e).  
 4 The vertical structure of the eddy flux variability indicates that there is a difference of nearly one order  
 5 of magnitude between 100 and 300 m depth. From that depth on, the eddy flux variability decreases  
 6 linearly.  
 7 In contrast with the northern boundary, the seasonal variability at the southern boundary peaks during  
 8 Austral Spring (Fig. 16d), in phase with the intraseasonal activity of the horizontal currents normal to  
 9 the section. The amplitude of the seasonal cycle is the largest around the depth of the oxycline, and  
 10 remains high down to the vicinity of the OMZ core upper limit (Fig. 16c). Below the depth of the OMZ  
 11 core, the amplitude of the EOF mode decreases sharply ( $\sim$ one order of magnitude in 100m; Fig. 16c).  
 12 This is evidenced by the profile of the eddy flux seasonal variability, estimated in the same manner as  
 13 for the northern boundary (Fig. 16e). This profile shares some characteristics with its counterpart at the  
 14 northern boundary, meaning, a sharp decrease between the oxycline and the OMZ core depths,  
 15 suffering a reduction of nearly 90% (Fig. 16e). On the other hand, the variability along the southern  
 16 boundary is  $\sim$ 70% larger than along the northern boundary. At both boundaries, the zonal wavelength  
 17 of the latitudinal variability is estimated to be of the order of  $\sim 10^2$  km, a scale that falls within the range  
 18 of observed eddies diameter (Chaigneau and Pizarro, 2005), which indicates that locally, eddies can  
 19 either inject or remove DO from the OMZ on average over a season. The mean oxygen eddy flux  
 20 across the boundaries is nevertheless positive.

21

## 22 **5 Discussion and concluding remarks**

23 A high resolution coupled physical/biogeochemical model experiment is used to document the seasonal  
 24 variability of the OMZ off Peru. The annual harmonic of DO reveals three main regions where DO  
 25 exhibits specific propagating characteristics and amplitude, suggesting distinct dynamical regimes: 1)  
 26 The coastal domain; 2) the offshore ocean below 400 m and 3) at the southern and northern boundaries.  
 27 In the coastal portion of the OMZ, the seasonal variability is related to the local wind forcing, and  
 28 therefore follows to a large extent the paradigm of upwelling triggered productivity, followed by  
 29 remineralization. It is shown in particular that the DO peaks in Austral winter which is associated with  
 30 mixing induced by both the increase in baroclinic instability and intraseasonal wind activity. This is





1 counter intuitive with regards to the seasonality of the alongshore upwelling favorable winds also  
2 peaking in Austral winter, which would favor the intrusion of deoxygenated waters from the open  
3 ocean OMZ to the shelf. Instead, the coastal domain can be viewed as a source of DO in Austral winter  
4 for the OMZ through offshore transport. The latter is induced by eddies that are triggered by the  
5 instabilities of the PUC. In the model, the offshore DO eddy flux has a marked seasonal cycle that is in  
6 phase with the seasonal cycle of the DO along the coast, implying that the coastal domain, viewed here  
7 as the eastern boundary of the OMZ, is a source of seasonal variability of the OMZ. This appears to  
8 operate effectively in the first 300 m. Below that depth, the DO eddy flux is much reduced due to both  
9 a much weaker eddy activity, and very low DO concentration. On the other hand, a mean seasonal DO  
10 flux is observed and exhibits propagating features reminiscent of the vertical propagation of energy  
11 associated with the annual extra tropical Rossby wave.

12 In the upper 300 m, the OMZ seasonal variability is also associated with the DO eddy flux at the OMZ  
13 meridional boundaries where it is the most intense. We find that, at the northern boundary, the seasonal  
14 cycle in DO eddy flux peaks in Austral winter, while it peaks a season later at the southern boundary.  
15 Additionally, the amplitude of the seasonal cycle in DO eddy flux is larger at the southern boundary  
16 than at the northern boundary. The schematics of Figure 17 summarize the main processes documented  
17 in this paper to explain the seasonality of the OMZ volume.

18 While previous studies have mostly focused on the role of the mean DO eddy flux in shaping the OMZ  
19 boundaries (Resplandy et al., 2012; Brandt et al., 2015; Bettencourt et al., 2015), we have documented  
20 here the seasonal variability in the DO eddy flux at the OMZ boundaries, including the “eastern  
21 boundary” formed by the coastal system. We infer that the seasonality of the DO eddy flux is  
22 controlled by distinct physical processes depending on the boundary: At the “eastern boundary”, there  
23 is a constructive coupling between eddies resulting from the instability of the PUC peaking in Austral  
24 winter, and the enhanced DO along the coast resulting from enhanced mixing at the same season. At  
25 the northern boundary of the OMZ, the DO eddy flux is also related to the strong EKE around 5°S that  
26 peaks in Austral winter. Whether or not the strong EKE found there results from the instability of the  
27 coastal current system or of the EUC and the South Equatorial Current (SEC), would need to be  
28 explored. Despite the fact that the OMZ northern boundary is embedded in the equatorial wave guide,  
29 since the intraseasonal Kelvin wave activity tends to peak in Austral summer (Illig et al., 2014) it can  
30 be ruled out that the seasonal cycle in DO eddy flux is strongly linked to the intraseasonal long





1 equatorial waves.  
2 Regarding the southern boundary, it is interesting to note that the DO eddy flux peaks in Austral spring,  
3 three months later than at the northern boundary. A possible mechanism driving the local variability  
4 observed at the southern section is the generation of local baroclinic instability and vorticity input from  
5 wind stress curl as observed for the California system (Kelly et al, 1998). The southern section lies  
6 within the northeast rim of the Southeast Pacific Anticyclone, and the seasonal cycle phase peak agrees  
7 with the reported intensity peak of the seasonal cycle of the Anticyclone, towards the end of the year  
8 (Rahn et al., 2015; Acapichun and Garcés-Vargas, 2015). In this sense, the mesoscale activity in this  
9 region could be directly modulated by the winds. Dewitte et al. (2008) also report that intraseasonal  
10 (internal) variability in currents can originate from the interactions between the annual extra tropical  
11 Rossby wave and the mean circulation in a medium resolution oceanic regional model over this region.  
12 The actual source of the eddy activity in this region would also deserve further investigation.  
13 Our study also reveals that the most prominent propagating features in DO inside the OMZ at annual  
14 frequency is below ~300 m, where the seasonal DO flux follows approximately the theoretical WKB  
15 ray paths of the annual ETRW. From that depth, we also show that the seasonal variability in physical  
16 fluxes becomes one order of magnitude larger than the one of the biogeochemical fluxes (Fig. 8c). This  
17 supports the observation that DO tends to behave as a passive tracer so that vertical displacements of  
18 the DO isopleths mimic those of the isotherms, inducing a seasonal DO flux that resembles the energy  
19 flux path of the ETRW. This mechanism adds a dimension to the understanding of the OMZ variability,  
20 considering that the vertical propagation of ETRW can take place at a wide range of frequencies  
21 (Ramos et al., 2008).  
22 We now discuss implications of our results with regards to current concerns around OMZ variability at  
23 long timescales. A recent study has suggested a trend in the OMZ towards expansion and  
24 intensification (Stramma et al., 2008) whose forcing mechanism remains unclear (Stramma et al.,  
25 2010). Observations in the Pacific Ocean also suggest that the OMZ characteristics vary decadal  
26 (Stramma et al., 2008; 2010). Since decadal variability can manifest as a low frequency modulation of  
27 the seasonal cycle, our study may provide guidance for investigating OMZ variability at long  
28 timescales. In particular we find that the amplitude of the seasonal cycle is nearly twice as large at the  
29 southern boundary than at the northern boundary and “coastal boundary”, which suggests a larger  
30 sensitivity of the OMZ variability at the southern boundary to the modulation of eddy activity by



1 climate forcing. This view would preferentially link the OMZ low frequency fluctuations to mid  
2 latitudes changes in the circulation. We note however that the relative contribution of the mean DO flux  
3 and the DO eddy flux exhibits significant interannual fluctuations at the boundaries (not shown), which  
4 suggests that eddy induced DO flux may not be the only key player for understanding long term trend  
5 in the OMZ. It is interesting to note that so far, it has been difficult to reconcile the observed trend in  
6 the OMZ with the trend simulated by the current generation of coupled models (Stramma et al., 2012),  
7 which has been attributed to biases in the mean circulation and inadequate remineralization  
8 representation (Cocco et al., 2013; Cabré et al., 2015). Our results support the view that such  
9 discrepancy may partly originate from the inability of the low resolution models to account for the DO  
10 eddy flux and its modulation. Regional modeling experiments also showed that eddy activity can be  
11 modulated at ENSO and decadal timescales (Combes et al., 2015; Dewitte et al., 2012). This issue  
12 would certainly require further investigation, and could benefit from the experimentation with our  
13 coupled model platform. This is planned for future work.

14

## 15 **Acknowledgments**

16 O. Vergara was supported by a doctoral scholarship from the National Chilean Research and  
17 Technology Council (CONICYT) through the program Becas Chile (scholarship 72130138). The  
18 authors are thankful for the financial support received from the Centre National d'Etudes Spatiales  
19 (CNES). During the preparation of this work O. Vergara was supported by a mobility scholarship from  
20 the University of Toulouse, through the ATUPS program when visiting the CEAZA. M. Ramos  
21 acknowledges support from FONDECYT (project 1140845) and Chilean Millennium Initiative  
22 (NC120030).



## 1 References

- 2 Acapichun, S. and Garcés-Vargas, J.: Variability of the Southeast Pacific Subtropical Anticyclone and  
 3 its impact on sea surface temperature off north-central Chile, *Cienc. Mar.*, 41, 1-20, doi:  
 4 10.7773/cm.v41i1.2338, 2015.
- 5 Arevalo-Martinez, D., Kock, L. A., Löscher, C. R., Schmitz, R. A., and Bange, R. A.: Massive nitrous  
 6 oxide emissions from the tropical South Pacific Ocean, *Nat. Geosci.*, doi: 10.1038/NGEO2469, 2015.
- 7 Bettencourt, J.H., López, C., Hernández-García, E., Montes, I., Sudre, J., Dewitte, B., Paulmier A., and  
 8 Garçon, V. : Boundaries of the Peruvian Oxygen Minimum Zone shaped by coherent mesoscale  
 9 dynamics, *Nat. Geosci.*, doi: 10.1038/ngeo2570, 2015.
- 10 Bianchi, D., Dunne, J. P., Sarmiento, J. L., and Galbraith, E. D.: Data-based estimates of suboxia,  
 11 denitrification, and N<sub>2</sub>O production in the ocean and their sensitivities to dissolved O<sub>2</sub>, *Global*  
 12 *Biogeochem. Cy.*, 26, GB2009, doi:10.1029/2011GB004209, 2012.
- 13 Brandt, P., Bange, H. W., Banyte, D., Dengler, M., Didwischus, S.-H., Fischer, T., Greatbatch, R. J.,  
 14 Hahn, J., Kanzow, T., Karstensen, J., Körtzinger, A., Krahmann, G., Schmidtko, S., Stramma, L.,  
 15 Tanhua, T., and Visbeck, M.: On the role of circulation and mixing in the ventilation of oxygen  
 16 minimum zones with a focus on the eastern tropical North Atlantic, *Biogeosciences*, 12, 489-512,  
 17 doi:10.5194/bg-12-489-2015, 2015.
- 18 Cabré, A., Marinov, I., Bernardello, R., and Bianchi, D.: Oxygen minimum zones in the tropical Pacific  
 19 across CMIP5 models: mean state differences and climate change trends, *Biogeosciences*, 12, 6525-  
 20 6587, doi:10.5194/bgd-12-6525-2015, 2015.
- 21 Cambon G., Goubanova, K., Marchesiello, P., Dewitte, B., Illig, S., and Echevin, V.: Assessing the  
 22 impact of downscaled winds on a regional ocean model simulation of the Humboldt system, *Ocean*  
 23 *Model.*, 65, 11-24, 2013.
- 24 Chavez, F. P., Bertrand, A., Guevara-Carrasco, R., Soler, P., and Csirke, J.: The northern Humboldt  
 25 Current System: Brief history, present status and a view towards the future, *Prog. Oceanogr.*, 79, pp.  
 26 95–105, 2008.
- 27 Chaigneau, A., and Pizarro, O.: Eddy characteristics in the eastern South Pacific, *J. Geophys. Res.*, 110,



- 1 C06005, doi:10.1029/2004JC002815, 2005.
- 2 Chaigneau, A., Eldin G., and Dewitte, B.: Eddy activity in the four major upwelling systems from  
 3 satellite altimetry (1992–2007), *Prog. Oceanogr.*, 83 (1–4), 117–123, doi:10.1016/j.pocean.2009.07.012,  
 4 2009.
- 5 Cocco, V., Joos, F., Steinacher, M., Frölicher, T. L., Bopp, L., Dunne, J., Gehlen, M., Heinze, C., Orr,  
 6 J., Oschlies, A., Schneider, B., Segschneider, J., and Tjiputra, J.: Oxygen and indicators of stress for  
 7 marine life in multi-model global warming projections, *Biogeosciences*, 10, 1849–1868,  
 8 doi:10.5194/bg-10-1849-2013, 2013.
- 9 Combes, V., Hormazabal, S., and Di Lorenzo, E.: Interannual variability of the subsurface eddy field in  
 10 the Southeast Pacific. *J. Geophys. Res.*, 120, 4907–4924, doi:10.1002/2014JC010265, 2015.
- 11 Cornejo, M., Farías, L., and Paulmier, A.: Temporal variability in N<sub>2</sub>O water content and its air-sea  
 12 exchange in an upwelling area off central Chile (36° S), *Mar. Chem.*, 101, 85–94,  
 13 doi:10.1016/j.marchem.2006.01.004, 2006.
- 14 Cornejo, M. and Farías, L.: Following the N<sub>2</sub>O consumption at the Oxygen Minimum Zone in the  
 15 eastern South Pacific, *Biogeosciences*, 9, 2691–2707, doi:10.5194/bgd-9-2691-2012, 2012.
- 16 Czeschel, R., Stramma, L., Schwarzkopf, F. U., Giese, B. S., Funk, A., and Karstensen, J.: Middepth  
 17 circulation of the eastern tropical South Pacific and its link to the oxygen minimum zone, *J. Geophys.*  
 18 *Res.*, 116, C01015, doi:10.1029/2010JC006565, 2011.
- 19 Czeschel, R., Stramma, L., Weller, R. A., and Fischer, T.: Circulation, eddies, oxygen and nutrient  
 20 changes in the eastern tropical South Pacific Ocean, *Ocean Sci.*, 11, 455–4703. doi:10.5194/os-11-455-  
 21 2015, 2015.
- 22 daSilva A., Young, A.C., and Levitus, S.: Atlas of surface marine data 1994. Algorithms and  
 23 procedures. vol. 1 Technical Report 6, US Department of Commerce, NOAA, NESDIS, 1994.
- 24 Dewitte B., Ramos, M., Echevin, V., Pizarro, O., and duPenhoat, Y.: Vertical structure variability in a  
 25 seasonal simulation of a medium-resolution regional model simulation of the South Eastern Pacific.  
 26 *Prog. Oceanogr.*, 79, 120–137, 2008.
- 27 Dewitte, B., Illig, S., Renault, L., Goubanova, K., Takahashi, K., Gushchina, D., Mosquera, K., and



- 1 Purca, S.: Modes of covariability between sea surface temperature and wind stress intraseasonal
- 2 anomalies along the coast of Peru from satellite observations (2000–2008), *J. Geophys. Res.*, 116,
- 3 C04028, doi:10.1029/2010JC006495, 2011.
- 4 Dewitte, B., Vazquez-Cuervo, J., Goubanova, K., Illig, S., Takahashi, K., Cambon, G., Purca, S.,
- 5 Correa, D., Gutierrez, D., Sifeddine, A., and Ortlieb, L.: Change in El Niño flavours over 1958–2008:
- 6 Implications for the long-term trend of the upwelling off Peru, *Deep Sea Res., Part II*, 77–80, 143–156,
- 7 doi:10.1016/j.dsr2.2012.04.011, 2012.
- 8 Dunn J. R., and Ridgway, K. R.: Mapping ocean properties in regions of complex topography, *Deep-*
- 9 *Sea Res. Pt.*, 49, 591–604, 2002.
- 10 Dunne, J. P., Armstrong, R. A., Gnanadesikan, A., and Sarmiento, J. L.: Empirical and mechanistic
- 11 models for the particle export ratio, *Global Biogeochem. Cy.*, 19, GB4026, doi:10.1029/2004gb002390,
- 12 2005.
- 13 Duteil, O. and Oschlies, A.: Sensitivity of simulated extent and future evolution of marine suboxia to
- 14 mixing intensity, *Geophys. Res. Lett.*, 38, L06607, doi:10.1029/2011GL046877, 2011.
- 15 Duteil, O., Schwarzkopf, F.U., Böning, C. W., and Oschlies, A.: Major role of the equatorial current
- 16 system in setting oxygen levels in the eastern tropical Atlantic Ocean: A high-resolution model study,
- 17 *Geophys. Res. Lett.*, 41, 2033–2040, doi:10.1002/2013GL058888, 2014.
- 18 Echevin, V., Aumont, O., Ledesma, J., and Flores, G.: The seasonal cycle of surface chlorophyll in the
- 19 Peruvian upwelling system: A modelling study. *Progr. Oceanogr.*, 79, 2–4, 167–176, 2008.
- 20 Eliassen, A., and Palm, E.: On the transfer of energy in stationary mountain waves. *Geophys. Publ.*, 22
- 21 (3), 1–23, 1960.
- 22 Farías, L., Paulmier, A., and Gallegos, M.: Nitrous oxide and N-nutrient cycling in the oxygen
- 23 minimum zone off northern Chile. *Deep Sea Research I* 54, 164–180. doi: 10.1016/j.dsr.2006.11.003,
- 24 2007.
- 25 Fuenzalida, R., Schneider, W., Garces-Vargas, J., Bravo, L., and Lange, C.: Vertical and horizontal
- 26 extension of the oxygen minimum zone in the eastern South Pacific Ocean, *Deep Sea Res., Part II*, 56,
- 27 992–1003, doi:10.1016/j.dsr2.2008.11.001, 2009.



- 1 Garcia, H. E. and Gordon, L. I.: Oxygen solubility in seawater – better fitting equations, *Limnol.*
- 2 *Oceanogr.*, 37, 1307–1312, 1992.
- 3 Goubanova, K., Echevin, V., Dewitte, B., Codron, F., Takahashi, K., Terray, P., and Vrac, M.: Statistical
- 4 downscaling of sea-surface wind over the Peru–Chile upwelling region: diagnosing the impact of
- 5 climate change from the IPSL-CM4 model. *Clim. Dyn.* DOI 10.1007/s00382-010-0824-0, 2011.
- 6 Gruber, N.: The marine nitrogen cycle: Overview of distributions and processes, in: *Nitrogen in the*
- 7 *marine environment*, second edition, Capone, D. G., Bronk, D. A., Mulholland, M. R. and Carpenter, E.
- 8 J., Eds., Elsevier, Amsterdam, 1-50, 2008.
- 9 Gruber, N., Lachkar, Z., Frenzel, H., Marchesiello, P., Münnich, M., McWilliams, J. C., Nagai, T., and
- 10 Plattner, G. K.: Eddy-induced reduction of biological production in eastern boundary upwelling
- 11 systems, *Nat. Geosci.*, 4, 787–792, doi:10.1038/NGEO01273, 2011.
- 12 Gutiérrez, D., Enriquez, E., Purca, S., Quipuzcoa, L., Marquina, R., Flores, G., Graco, M.: Oxygenation
- 13 episodes on the continental shelf of central Peru: remote forcing and benthic ecosystem response. *Prog.*
- 14 *Oceanogr.* 79, 177–189, 2008.
- 15 Gutiérrez D., Bouloubassi, I., Sifeddine, A., Purca, S., Goubanova, K., Graco, M., Field, D., Mejanelle,
- 16 L., Velazco, F., Lorre, A., Salvatelli, R., Quispe, D., Vargas, G., Dewitte, B., and Ortlieb, L.: Coastal
- 17 cooling and increased productivity in the main upwelling zone off Peru since the mid-twentieth century.
- 18 *Geophys. Res. Lett.*, 38, L07603, doi:10.1029/2010GL046324, 2011.
- 19 Gutknecht, E., Dadou, I., Le Vu, B., Cambon, G., Sudre, J., Garçon, V., Machu, E., Rixen, T., Kock, A.,
- 20 Flohr, A., Paulmier, A., and Lavik, G.: Coupled physical/biogeochemical modeling including O<sub>2</sub>-
- 21 dependent processes in Eastern Boundary Upwelling Systems: Application in the Benguela,
- 22 *Biogeosciences*, 10, 3559–3591, doi:10.5194/bg-10-1-2013, 2013a.
- 23 Gutknecht, E., Dadou, I., Marchesiello, P., Cambon, G., Le Vu, B., Sudre, J., Garçon, V., Machu, E.,
- 24 Rixen, T., Kock, A., Flohr, A., Paulmier, A., and Lavik, G.: Nitrogen transfers off Walvis Bay: A 3-D
- 25 coupled physical/biogeochemical modeling approach in the Namibian Upwelling System,
- 26 *Biogeosciences*, 10, 4117–4135, doi:10.5194/bg-10-4117-2013, 2013b.
- 27 Henley, B. J., Gergis, J., Karoly, D. J., Power, S. B., Kennedy, J., and Folland, C. K.: A Tripole Index
- 28 for the Interdecadal Pacific Oscillation. *Clim. Dyn.* , 45, 3077-3090, doi:10.1007/s00382-015-2525-1,



- 1 2015.
- 2 Henson, S. A., Sanders, R., and Madsen, E.: Global patterns in efficiency of particulate organic carbon
- 3 export and transfer to the deep ocean, *Global Biogeochem. Cy.*, 26, GB1028,
- 4 doi:10.1029/2011gb004099, 2012.
- 5 Illig, S., Dewitte, B., Goubanova, K., Cambon, G., Boucharel, J., Monetti, F., Romero, C., Purca S.,
- 6 and Flores, R.: Forcing mechanisms of intraseasonal SST variability off central Peru in 2000– 2008, *J.*
- 7 *Geophys. Res.*, 119, 3548–3573, doi:10.1002/ 2013JC009779, 2014.
- 8 Karstensen, J., Stramma, L., and Visbeck, M.: Oxygen minimum zones in the eastern tropical Atlantic
- 9 and Pacific oceans. *Progr. Oceanogr.* 77.4: 331-350, 2008.
- 10 Karstensen, J., Fiedler, B., Schütte, F., Brandt, P., Körtzinger, A., Fischer, G., Zantopp, R., Hahn, J.,
- 11 Visbeck, M., and Wallace, D.: Open ocean dead zones in the tropical North Atlantic Ocean,
- 12 *Biogeosciences*, 12, 2597-2605, doi:10.5194/bg-12-2597-2015, 2015.
- 13 Kelly, K., Beardsley, R., Limeburner, R., and Brink, K.: Variability of the near-surface eddy kinetic
- 14 energy in the California Current based on altimetric, drifter and moored data. *Journal Geophysical*
- 15 *Research* 103, 13,067–13,083, 1998.
- 16 Law, C. S., Brévière, E., de Leeuw, G., Garçon, V., Guieu, C., Kieber, D. J., Konradowitz, S.,
- 17 Paulmier, A., Quinn, P. K., Saltzman, E. S., Stefels, J., and von Glasow, R.: Evolving research
- 18 directions in Surface Ocean - Lower Atmosphere (SOLAS) science, *Environ. Chem.*, 10, 1-16, doi:
- 19 10.1071/EN12159, 2013.
- 20 Libes, S.M.: *An Introduction to Marine Biogeochemistry*, John Wiley and Sons, New York, 734pp,
- 21 1992.
- 22 Llanillo, P. J., Karstensen, J., Pelegrí, J. L., and Stramma, L.: Physical and biogeochemical forcing of
- 23 oxygen and nitrate changes during El Niño/El Viejo and La Niña/La Vieja upper-ocean phases in the
- 24 tropical eastern South Pacific along 86° W, *Biogeosciences*, 10, 6339-6355, doi: 10.5194/bg-10-6339-
- 25 2013, 2013.
- 26 Luyten, J.R., Pedlosky, J., and Stommel, H.: The ventilated thermocline. *Journal of Physical*
- 27 *Oceanography* 13, 292–309, 1983.



- 1 McClain, C. R., Cleave, M. L., Feldman, G. C., Gregg, W. W., Hooker, S. B., and Kuring, N.: Science  
2 quality SeaWiFS data for global biosphere research, *Sea Technol.*, 39, 9, 10–16, 1998.
- 3 Montes, I., Colas, F., Capet, X., and Schneider, W.: On the pathways of the equatorial subsurface  
4 currents in the Eastern Equatorial Pacific and their contributions to the Peru-Chile Undercurrent, *J.*  
5 *Geophys. Res.*, 115, C09003, doi:10.1029/2009JC005710, 2010.
- 6 Montes, I., Dewitte, B., Gutknecht, E., Paulmier, A., Dadou, I., Oschlies, A., and Garçon, V.: High-  
7 resolution modeling of the Eastern Tropical Pacific oxygen minimum zone: Sensitivity to the tropical  
8 oceanic circulation, *J. Geophys. Res. Oceans*, 119, doi:10.1002/2014JC009858, 2014.
- 9 Morales, C. E., Hormazabal, S. E., and Blanco, J.: Interannual variability in the mesoscale distribution  
10 of the depth of the upper boundary of the oxygen minimum layer off northern Chile (18–24S):  
11 Implications for the pelagic system and biogeochemical cycling, *J. Mar. Res.*, 57, 909–932,  
12 doi:10.1357/002224099321514097, 1999.
- 13 Morel, A., and Berthon, J. F.: Surface pigments, algal biomass profiles, and potential production of  
14 euphotic layer: Relationship reinvestigated in view of remote-sensing applications, *Limnol. Oceanogr.*,  
15 34, 1545–1562, 1989.
- 16 Nagai, T., Gruber, N., Frenzel, H., Lachkar, Z., McWilliams, J. C., and Plattner, G.-K.: Dominant role  
17 of eddies and filaments in the offshore transport of carbon and nutrients in the California Current  
18 System, *J. Geophys. Res. Oceans*, 120, 5318–5341, doi:10.1002/2015JC010889, 2015.
- 19 O'Reilly, J. E., Maritorena, S., Siegel, D., O'Brien, M. O., Toole, D., Mitchell, B. G., Kahru, M.,  
20 Chavez, F., Strutton, P. G., Cota, G. F., Hooker, S. B., McClain, C., Carder, K., Muller-Karger, F.,  
21 Harding, L., Magnuson, A., Phinney, D., Moore, G., Aiken, J., Arrigo, K. R., Letelier, R. M., and  
22 Culver, M.: Ocean chlorophyll a algorithms for SeaWiFS, OC2, and OC4: Version 4, in: *SeaWiFS*  
23 *Postlaunch Calibration and Validation Analyses, Part 3*, NASA Tech. Memo 2000–206892, vol. 11,  
24 Hooker, B., and Firestone, E. R., Eds., pp. 9–19, NASA, Goddard Space Flight Center, Greenbelt,  
25 Maryland, 2000.
- 26 Paulmier, A., and Ruiz-Pino, D.: Oxygen minimum zones (OMZs) in the modern ocean, *Prog.*  
27 *Oceanogr.*, 80, 3–4, 113–128, doi:10.1029/j.pcean.2008.08.001, 2009.
- 28 Paulmier, A., Ruiz-Pino, D., Garçon, V., and Farias, L.: Maintaining of the East South Pacific Oxygen

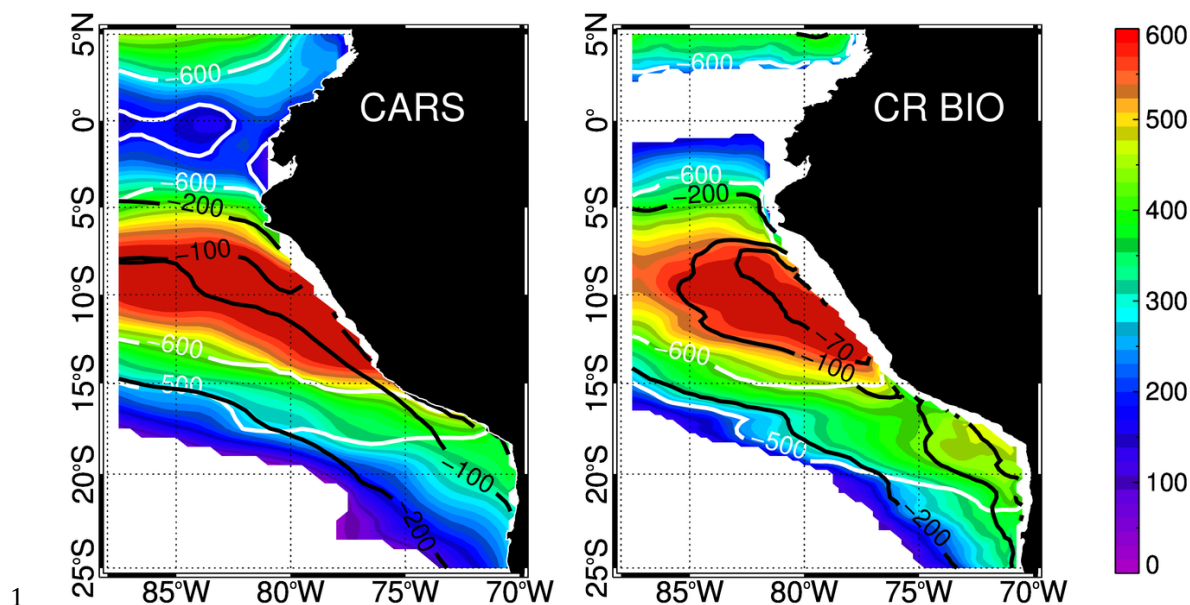




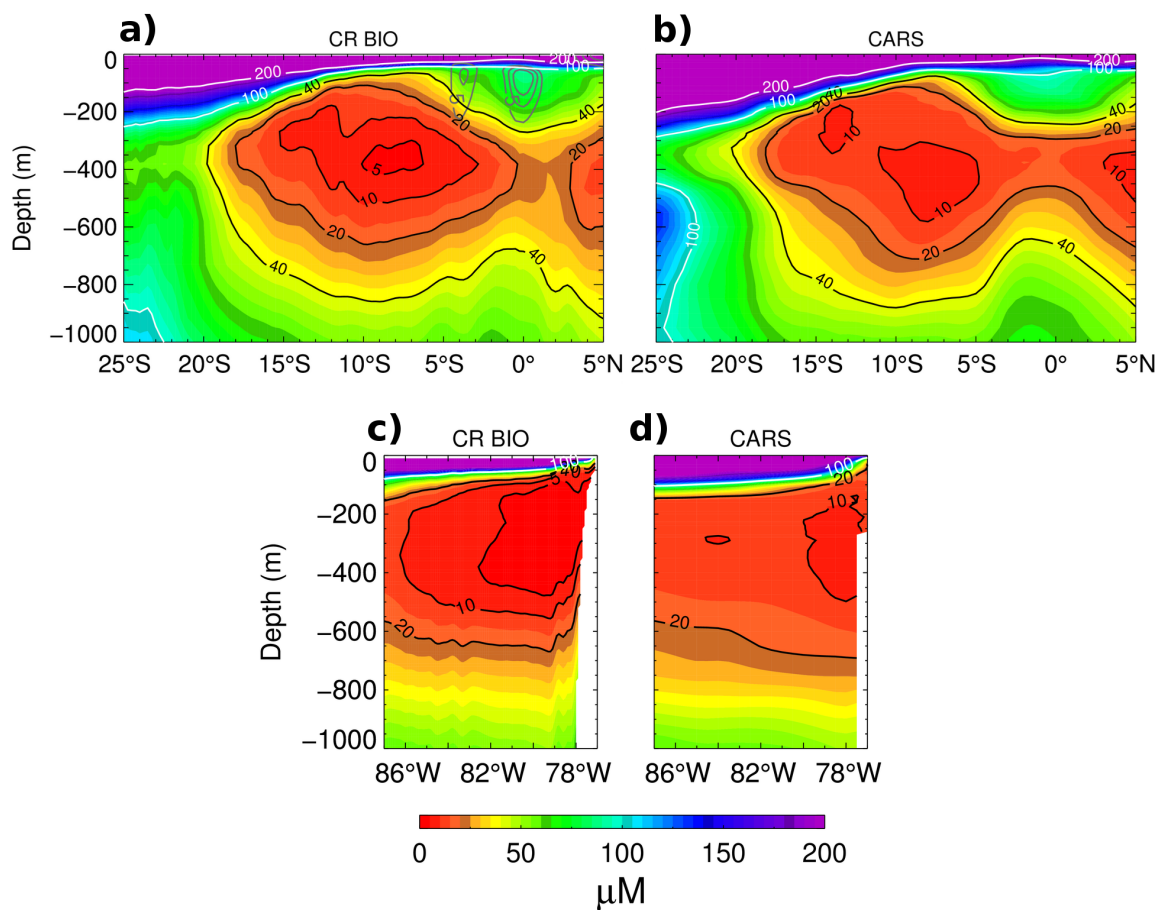
- 1 Minimum Zone (OMZ) off Chile, *Geophys. Res. Lett.*, 33, L20601, doi:10.1029/2006GL026801, 2006.
- 2 Paulmier, A., Ruiz-Pino, D., and Garçon, V.: The Oxygen Minimum Zone (OMZ) off Chile as intense
- 3 source of CO<sub>2</sub> and N<sub>2</sub>O, *Contin. Shelf Res.*, 28, 2746–2756, 2008.
- 4 Paulmier, A., Ruiz-Pino, D., and Garçon, V.: CO<sub>2</sub> maximum in the oxygen minimum zone (OMZ),
- 5 *Biogeosciences*, 8, 239–252, doi:10.5194/bg-8-239-2011, 2011.
- 6 Penven, P., Echevin, V., Pasapera, J., Colas, F., and Tam, J.: Average circulation, seasonal cycle, and
- 7 mesoscale dynamics of the Peru Current System: a modeling approach. *J. Geophys. Res.*, 110, C10021,
- 8 2005.
- 9 Pizarro, O., Shaffer, G., Dewitte, B., and Ramos, M.: Dynamics of seasonal and interannual variability
- 10 of the Peru-Chile Undercurrent, *Geophys. Res. Lett.*, 29(12), 1581, doi: 10.1029/2002GL014790, 2002.
- 11 Rahn, D., Rosenblüth, B., and Rutllant, J.: Detecting Subtle Seasonal Transitions of Upwelling in
- 12 North-Central Chile. *J. Phys. Oceanogr.*, 45, 854–867, 2015
- 13 Ramos, M., Dewitte, B., Pizarro, O., and Garric, G.: Vertical propagation of extratropical Rossby
- 14 waves during the 1997 – 1998 El Niño off the west coast of South America in a medium-resolution
- 15 OGCM simulation, *J. Geophys. Res.*, 113, C08041, doi:10.1029/2007JC004681, 2008.
- 16 Resplandy, L., Lévy, M., Bopp, L., Echevin, V., Pous S., Sarma, V. V. S. S., and Kumar, D.: Controlling
- 17 factors of the oxygen balance in the Arabian Sea's OMZ, *Biogeosciences*, 9, 5095–5109,
- 18 doi:10.5194/bg-9-5095-2012, 2012.
- 19 Richter I.: Climate model biases in the eastern tropical oceans: causes, impacts and ways forward.
- 20 *WIREs Clim Change* doi: 10.1002/wcc.338., 2015.
- 21 Ridgway K. R., Dunn, J.R., and Wilkin, J. L.: Ocean interpolation by four-dimensional least squares
- 22 -Application to the waters around Australia, *J. Atmos. Ocean. Tech.*, Vol 19, No 9, 1357–1375, 2002.
- 23 Shchepetkin, A. F. and McWilliams, J. C.: The regional oceanic modeling system: a split-explicit, free-
- 24 surface, topography-following-coordinate ocean model. *Ocean Model.* 9, 347–404, 2005.
- 25 Shchepetkin, A. F. and McWilliams, J. C.: Correction and commentary for “Ocean forecasting in
- 26 terrain-following coordinates: Formulation and skill assessment of the regional ocean modeling
- 27 system” by Haidvogel et al., *J. Comp. Phys.*, 227, 3595–3624, 2009.



- 1 Stramma, L., Johnson, G. C., Sprintall, J., and Mohrholz, V.: Expanding oxygen-minimum zones in the  
2 tropical oceans, *Science*, 320, 655–658, 2008.
- 3 Stramma, L., Johnson, G. C., Firing, E., and Schmidtko, S.: Eastern Pacific oxygen minimum zones:  
4 Supply paths and multidecadal changes, *J. Geophys. Res.*, 115, C09011, doi:10.1029/2009JC005976,  
5 2010.
- 6 Stramma, L., Oschlies, A., and Schmidtko, S.: Mismatch between observed and modeled trends in  
7 dissolved upper-ocean oxygen over the last 50 yr, *Biogeosciences*, 9, 4045–4057, doi:10.5194/bg-9-  
8 4045-2012, 2012.
- 9 Stramma, L., Bange, H. W., Czeschel, R., Lorenzo, A., and Frank, M.: On the role of mesoscale eddies  
10 for the biological productivity and biogeochemistry in the eastern tropical Pacific off Peru,  
11 *Biogeosciences*, 10, 7293–7306, doi:10.5194/bg-10-7293-2013, 2013.
- 12 Stramma, L., Weller, R. A., Czeschel, R., and Bigorre, S.: Eddies and an extreme water mass anomaly  
13 observed in the eastern south Pacific at the Stratus mooring, *J. Geophys. Res. Oceans*, 119, 1068–1083,  
14 2014.

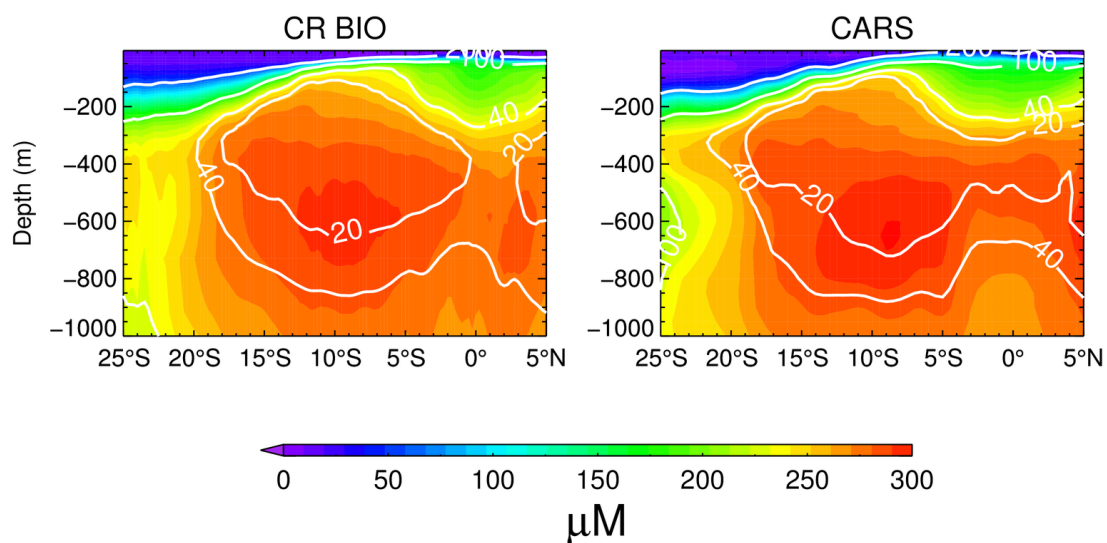


1  
 2  
 3 Figure 1. Mean Oxygen Minimum Zone core thickness (color scale in meters) for CARS and the  
 4 simulation. Depth of the lower (white) and upper (black) limits of the OMZ core are also depicted. The  
 5 OMZ core is defined as  $[DO] < 20 \mu M$ .



1  
2

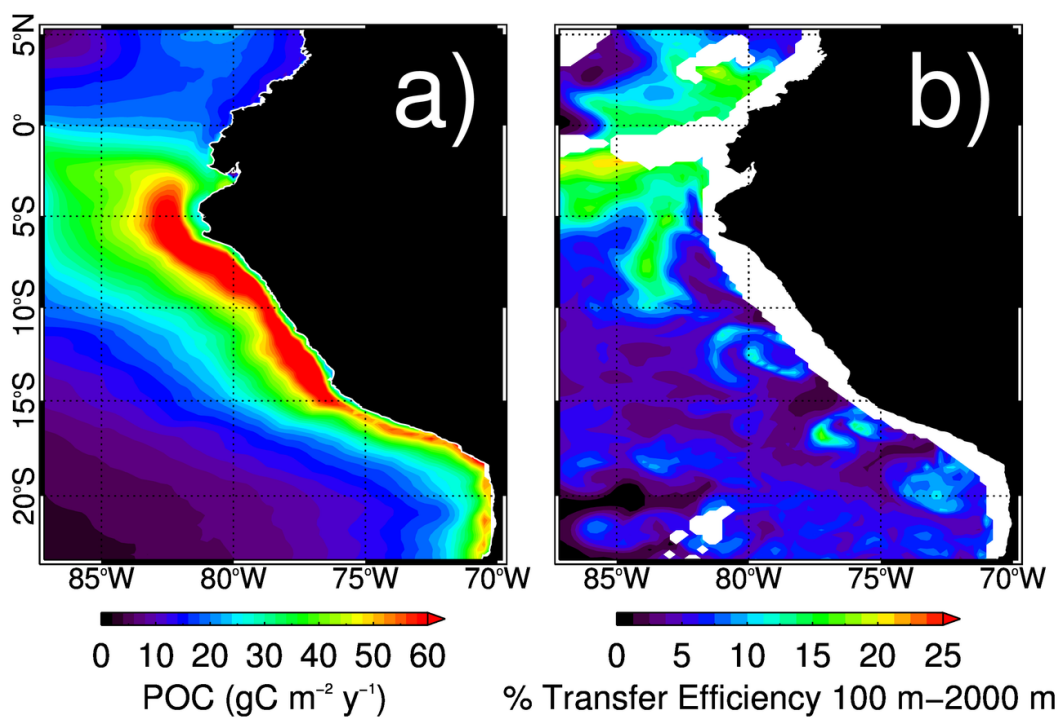
3 Figure 2. Mean oxygen concentration for a meridional section at 85°W (a and b) and a cross shore  
 4 section at 12°S (c and d), for both the simulation and CARS. Gray contours in (a) show zonal speed of  
 5 5, 10 and 15 cm s<sup>-1</sup> respectively.



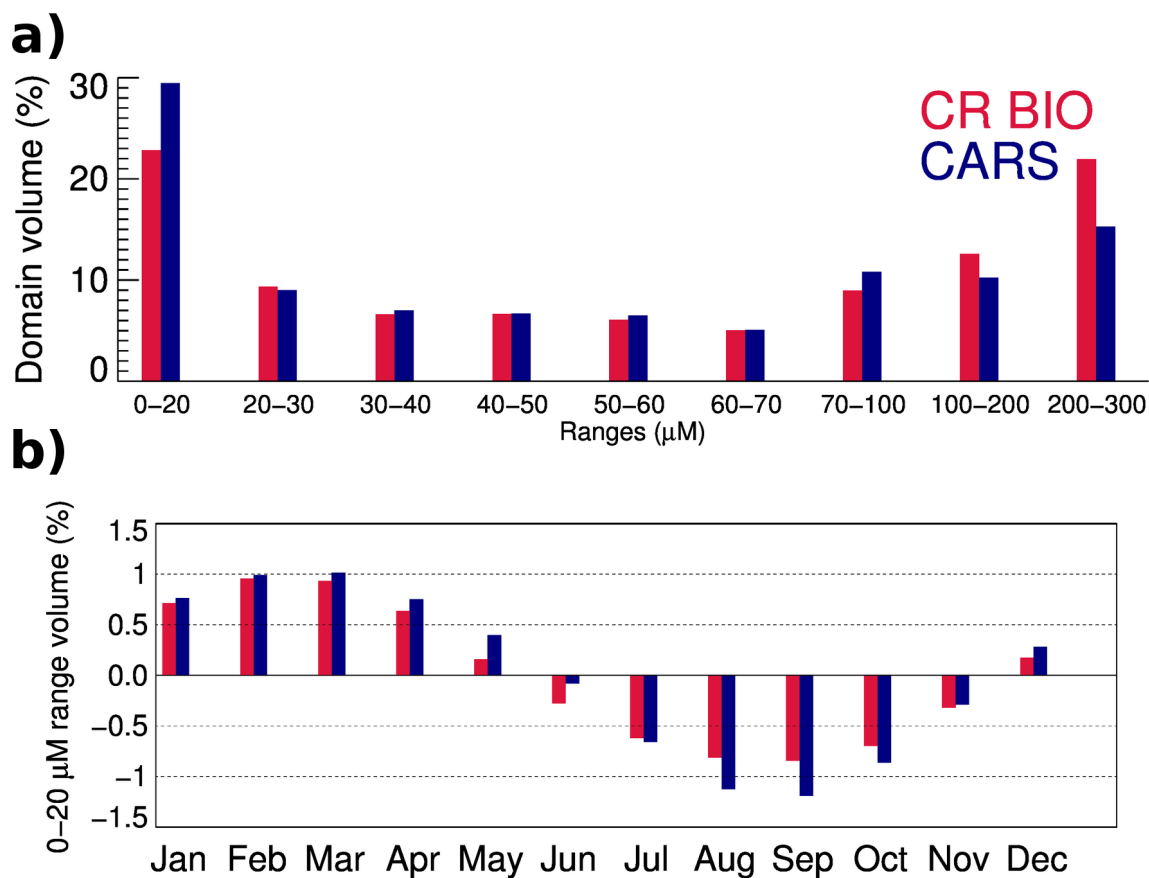
1

2

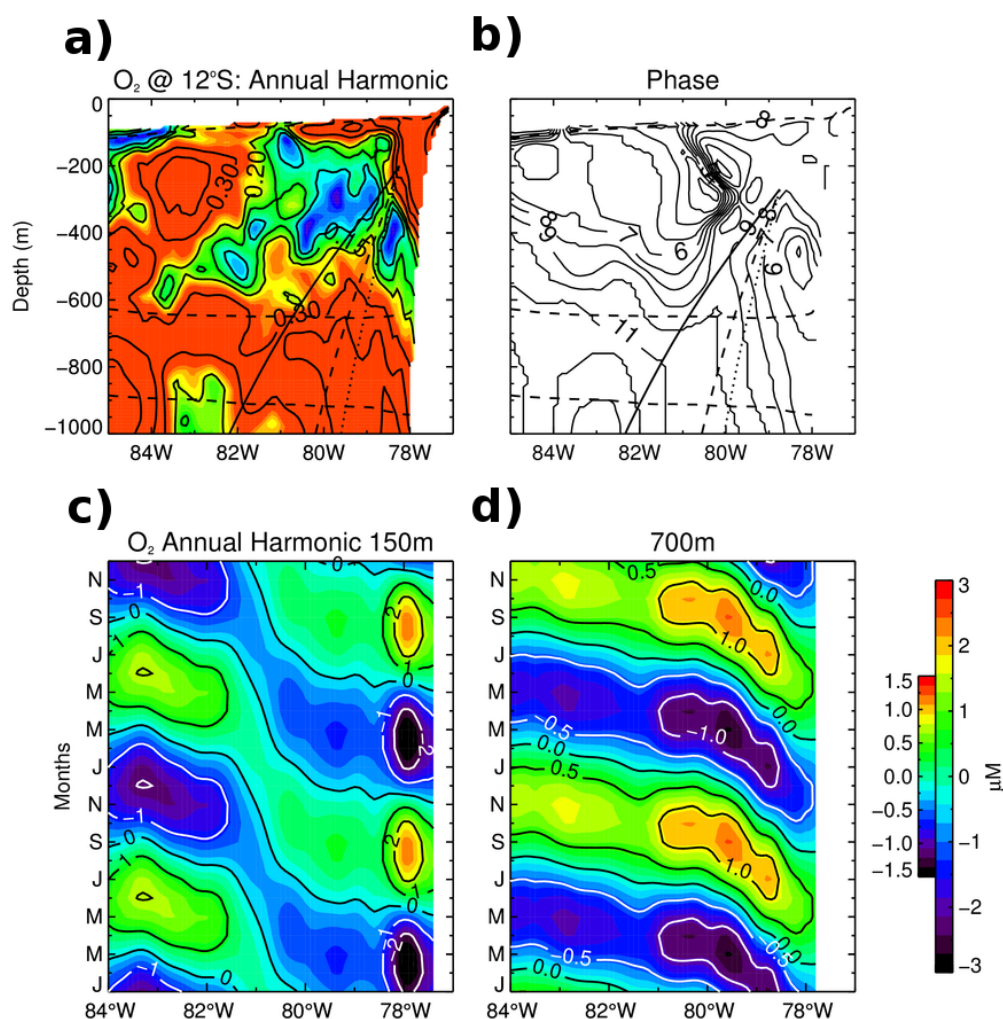
3 Figure 3. Mean Apparent Oxygen Utilization (AOU) at 85°W for both CR BIO and CARS. White  
 4 contours denote the mean oxygen concentration isopleths (in  $\mu\text{M}$ ).



1  
 2  
 3 Figure 4. (a) Particulate Organic Carbon (POC) flux at 100 m and (b) POC transfer efficiency between  
 4 100 m and 2000 m (POC flux at 2000 m divided by POC flux at 100 m), computed from the  
 5 simulation. Total flux at 100 m depth:  $0.8 \text{ Pg C year}^{-1}$ .



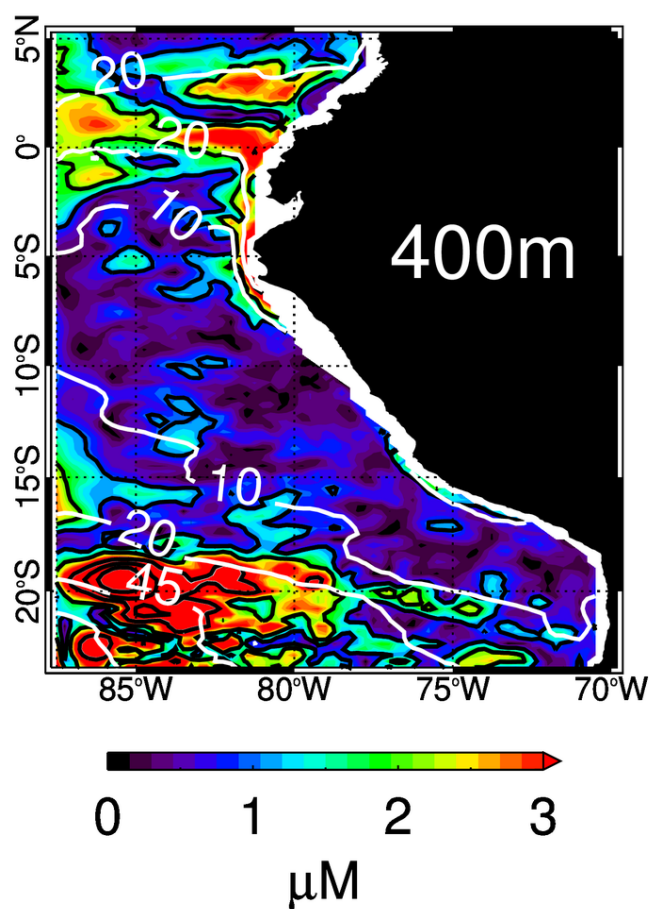
1  
 2  
 3 Figure 5. (a) Domain volume distribution ( $25^{\circ}\text{S}$ – $5^{\circ}\text{N}$ ,  $88^{\circ}\text{W}$ – $70^{\circ}\text{W}$ ) as a function of the oxygen  
 4 concentration, and (b) annual cycle, relative to the mean, of the volume distribution inside the OMZ  
 5 core (DO value range correspondig to 0–20  $\mu\text{mol L}^{-1}$ ), for both CARS and the simulation.



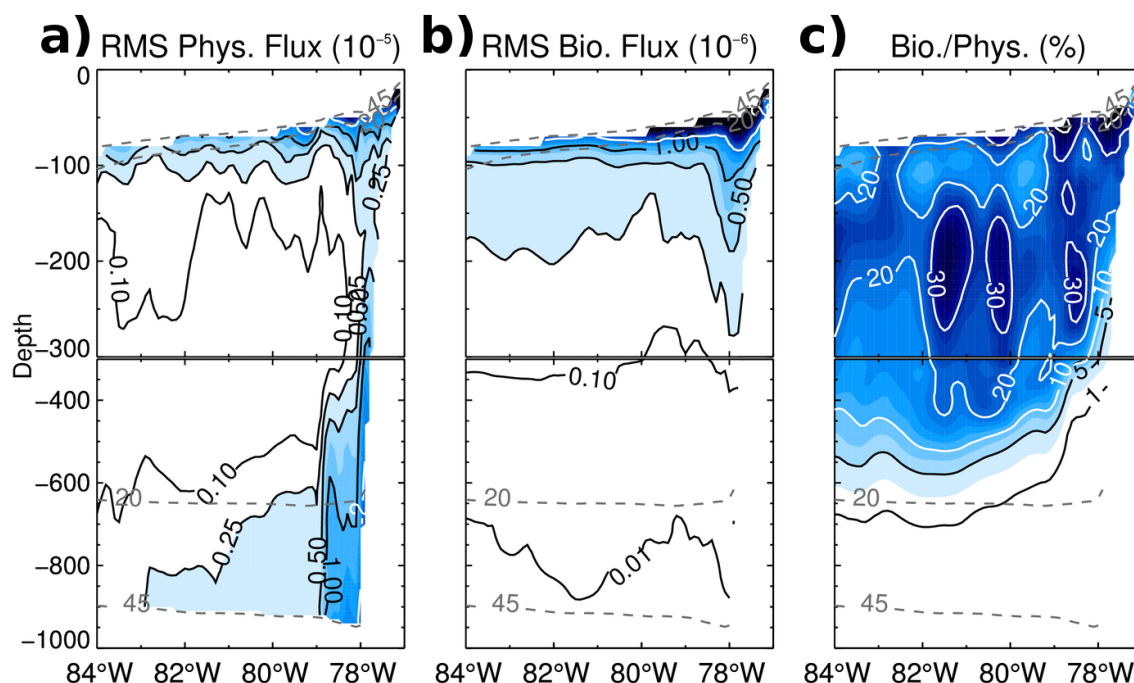
1  
2

3 Figure 6. Amplitude (a) and phase (b) of the annual harmonic of the normalized oxygen concentration  
 4 at 12°S. The slanted vertical lines show the theoretical WKB raypaths for the first (full), second  
 5 (dashed) and third (dotted) baroclinic modes (1 year period) of a long Rossby wave. Dashed contours  
 6 in (a) and (b) depict the 45 and 20  $\mu\text{M}$  mean oxygen values. (c) Annual harmonic of the Oxygen  
 7 concentration at 12°S, at 150 m and (d) 700 m depth. Small color scale corresponds to 700 m and the  
 8 large color scale denotes the levels used in (c).



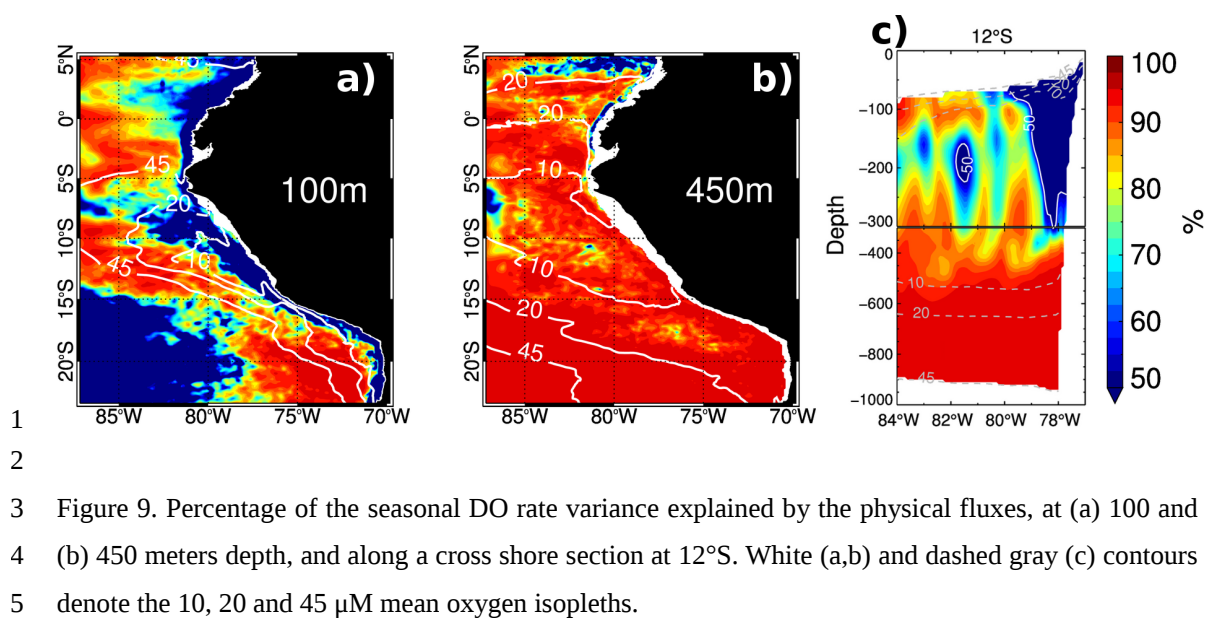


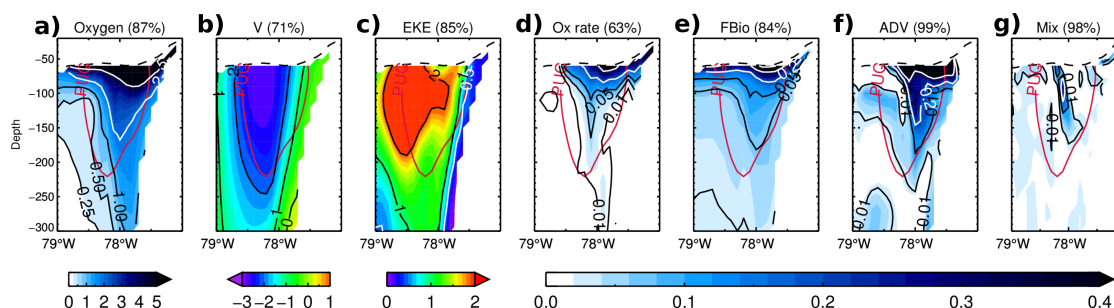
1  
 2  
 3 Figure 7. Annual DO harmonic amplitude at 400 meters depth. White contours denote the 10, 20 and  
 4 45  $\mu\text{M}$  mean oxygen isolines. Black contours denote the 1, 2, 4, 6 and 8  $\mu\text{M}$  levels.



1  
2

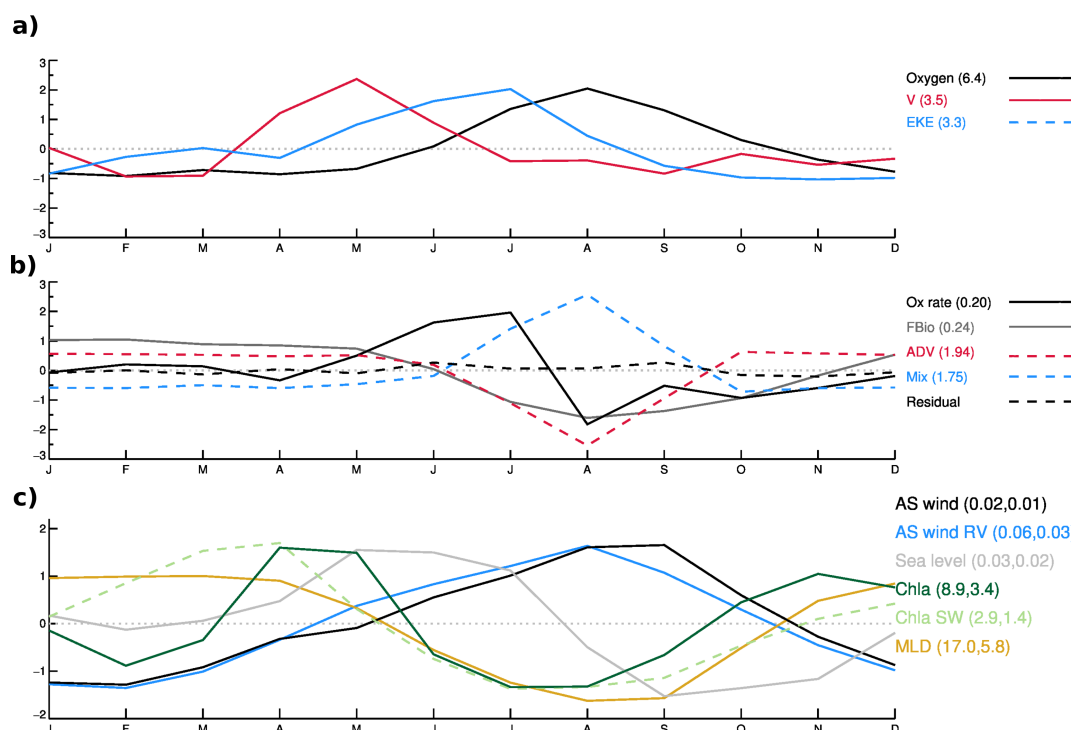
3 Figure 8. Root mean square of the seasonal cycle of (a) Physical and (b) Biogeochemical oxygen fluxes  
 4 (in  $10^{-5} \mu\text{M s}^{-1}$  and  $10^{-6} \mu\text{M s}^{-1}$ , respectively) for CR BIO at  $12^{\circ}\text{S}$ . c) Ratio between the RMS of the  
 5 biogeochemical fluxes and the physical fluxes, expressed as percentage. Dashed contours depict the 45  
 6 and  $20 \mu\text{M}$  mean oxygen values. Note the vertical scale change at 300m depth.





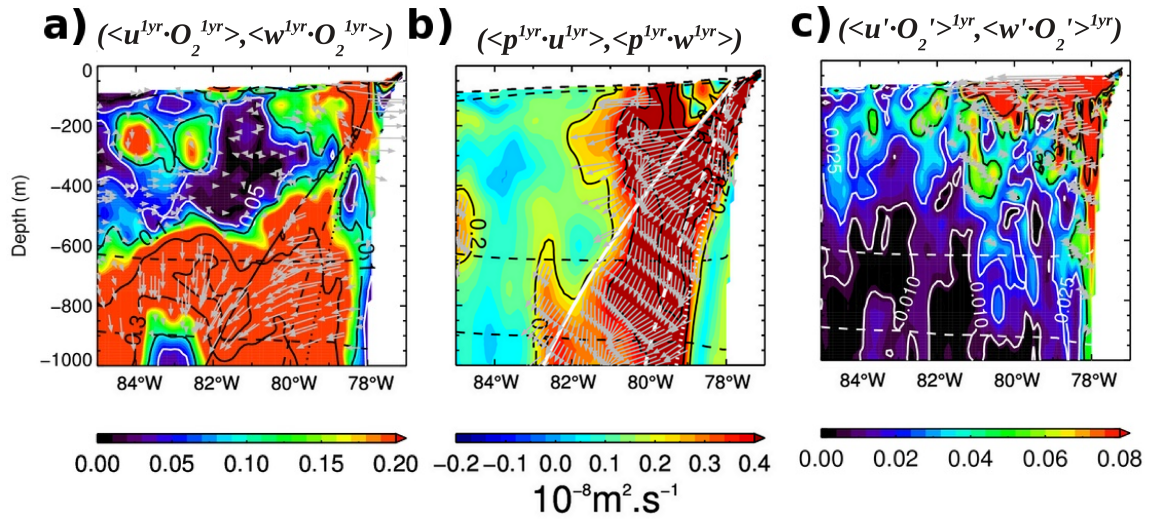
1  
2

3 Figure 10. Dominant climatological EOF modes (and percentage of explained variance): (a) oxygen  
 4 concentration (in  $\mu\text{M}$ ), (b) meridional currents (in  $\text{cm s}^{-1}$ ), (c) eddy kinetic energy (in  $\text{cm}^2 \text{s}^{-2}$ ), (d)  
 5 oxygen rate (in  $10^{-5} \mu\text{M s}^{-1}$ ), (e) biogeochemical flux (in  $10^{-5} \mu\text{M s}^{-1}$ ), (f) advective terms (including  $u, v$   
 6 and  $w$ , in  $10^{-5} \mu\text{M s}^{-1}$ ) and (g) mixing term (in  $10^{-5} \mu\text{M s}^{-1}$ ) for CR BIO at  $12^\circ\text{S}$ . Red contour denotes the  
 7 Peru Under Current ( $4 \text{ cm s}^{-1}$  southwards). Dashed contour depicts the  $45 \mu\text{M}$  isopleth.

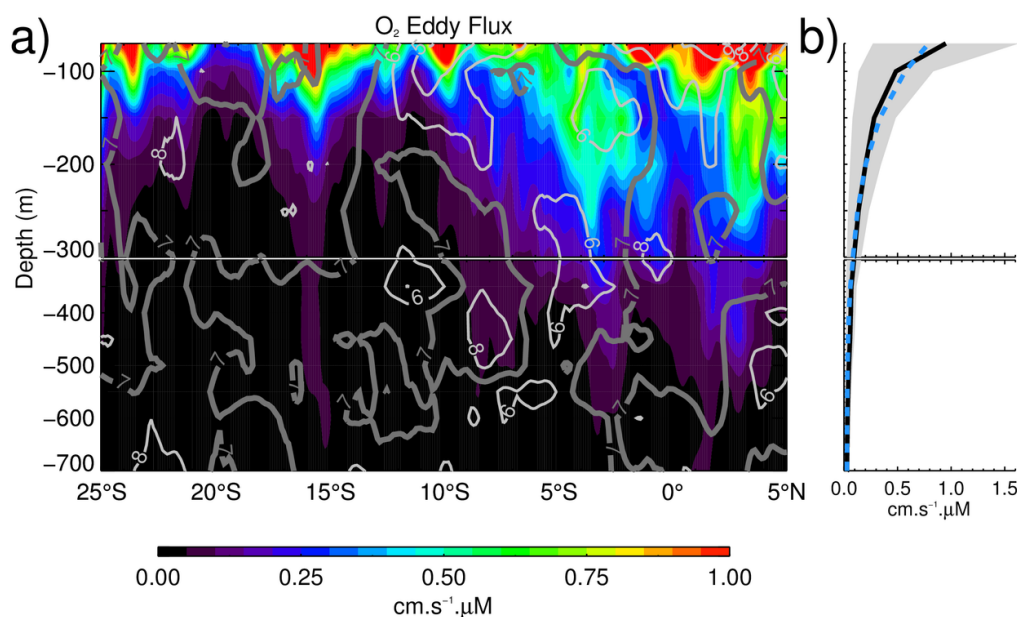


1  
2

3 Figure 11. Principal components associated to the EOF modes in Figure 10 (a and b). Residual  
 4 corresponds to the difference between Ox rate and the sum of the other oxygen budget terms.  
 5 Multiplying the principal components with the RMS (indicated in parenthesis) yields the seasonal cycle  
 6 with the same units as in Figure 10. (c) Normalized seasonal cycle of: coastal alongshore wind,  
 7 alongshore wind Running Variance (variance over a 30 day running window), coastal sea level, surface  
 8 chlorophyll-a from CR BIO, surface chlorophyll-a from SeaWifs and Mixed Layer Depth. Mean and  
 9 RMS used to normalize each time series, are indicated in parenthesis. Original seasonal cycle is found  
 10 by multiplying the normalized series by its RMS and then adding the mean. Original units are  $\text{N m}^{-2}$ ,  $\text{m}$ ,  
 11  $\text{mg m}^{-3}$ , and  $\text{m}$  respectively.



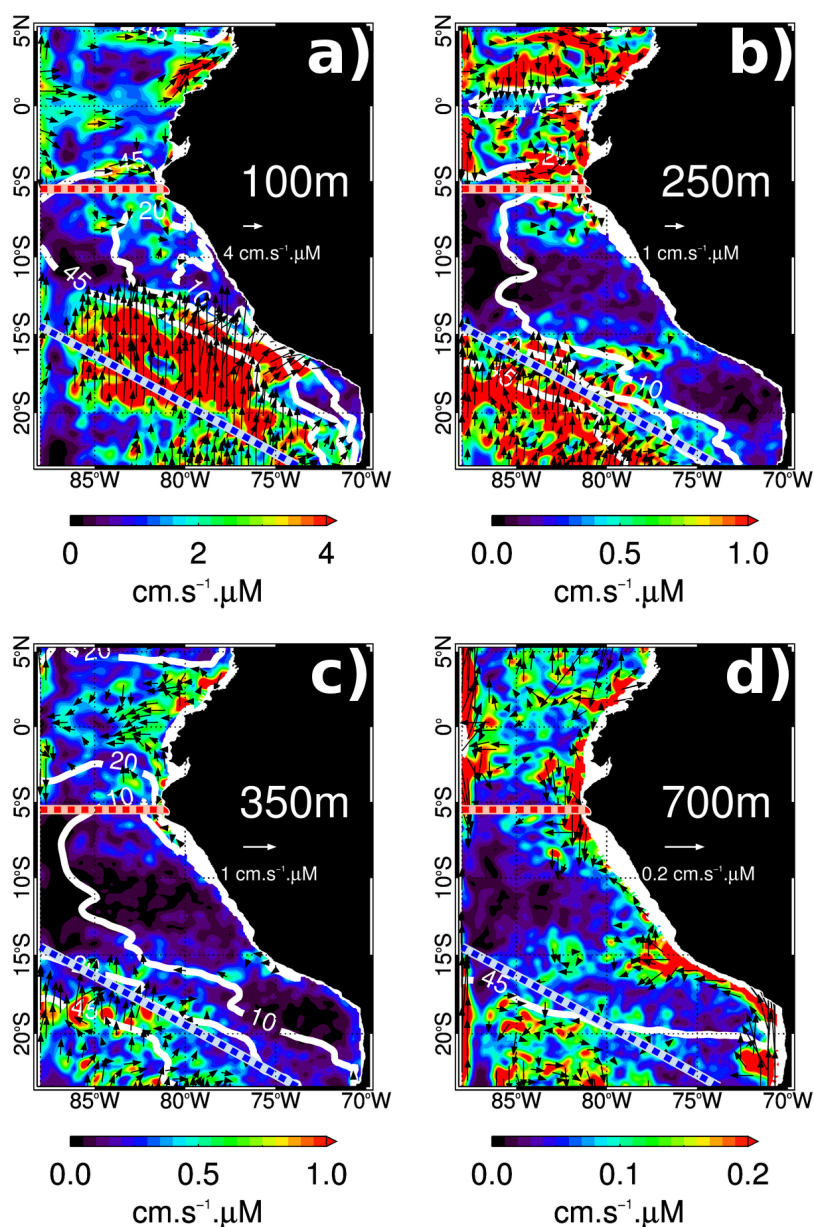
1  
 2  
 3 Figure 12. (a) Contribution of the annual harmonic to the oxygen flux vector ( $\langle u^{1yr} \cdot O_2^{1yr} \rangle, \langle w^{1yr} \cdot O_2^{1yr} \rangle$ ),  
 4 scaled by  $10^6$ , for a cross shore section at  $12^\circ\text{S}$ . Arrows indicate the vector direction. (b) Contribution  
 5 of the annual harmonic to energy flux vector ( $\langle p^{1yr} \cdot u^{1yr} \rangle, \langle p^{1yr} \cdot w^{1yr} \rangle$ ), in  $10^{-8} \text{ m}^2 \text{ s}^{-1}$ . Arrows inside the 0.2  
 6 contour indicate the vector direction. (c) Annual harmonic amplitude of the climatological oxygen eddy  
 7 flux vector ( $\langle u' \cdot O_2' \rangle^{1yr}, \langle w' \cdot O_2' \rangle^{1yr}$ ). Arrows indicate the vector direction. The apostrophes denote the  
 8 intraseasonal anomaly. Theoretical WKB raypaths (1 year period) originating from near the coast at the  
 9 surface for phase speed values of a first (full), second (dashed) and third (dotted) baroclinic modes are  
 10 shown in panels (a) and (b). Dashed contours indicate the 45 and 20  $\mu\text{M}$  oxygen isopleths (a, b, and c).  
 11 DO has been normalized by the variance of its climatology in (a) and (c) in order to emphasize flux  
 12 patterns where DO concentration is low.



1  
2

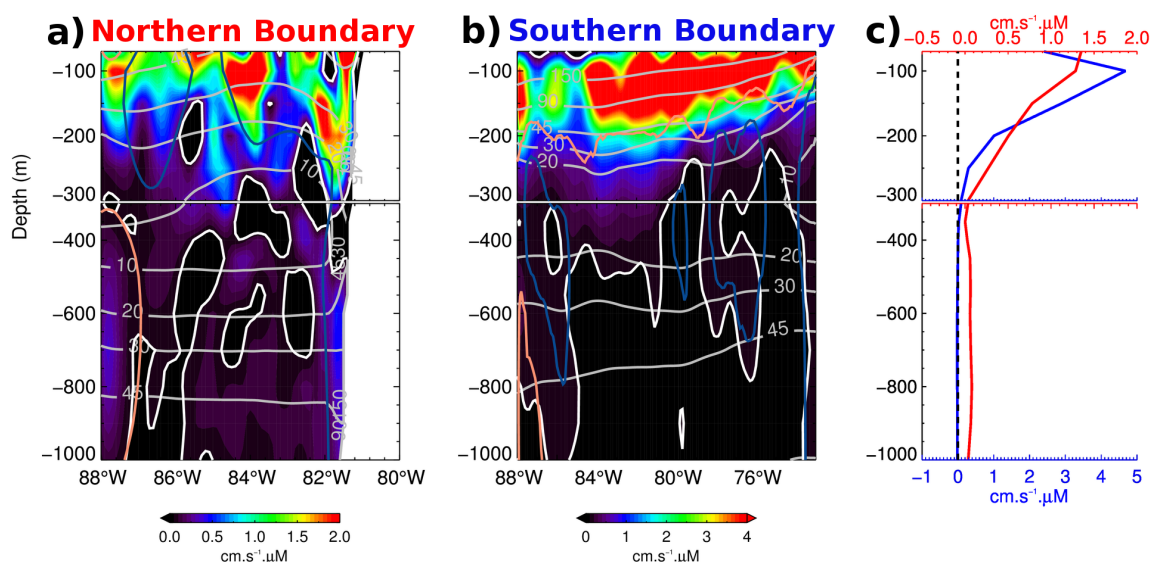
3 Figure 13. (a) Amplitude (color shading) and phase (months, gray contours) of the annual harmonic of  
 4 the climatological eddy oxygen flux along the coast. The climatology in oxygen eddy flux was  
 5 averaged over a coastal fringe of 2° width starting from 1° from the coast. (b) Meridional average  
 6 vertical profile (black line), average profile  $\pm$  RMS (gray shading). An exponential model fitted to the  
 7 average vertical profile (dashed blue line) yields a vertical decay scale of  $\sim 90$  m.





1  
 2  
 3 Figure 14. Module of the mean oxygen eddy flux vector ( $u'O_2', v'O_2'$ ) at (a) 100 m, (b) 250 m, (c) 350  
 4 m and (d) 700 m depth. Arrows -displayed only for values above the central value in each colorbar-  
 5 denote the vector direction. White contours correspond to the 45, 20 and 10  $\mu\text{M}$ . Red and blue lines  
 6 denote the position of vertical sections.





1

2

3 Figure 15. (a) Mean oxygen eddy flux normal to the section denoted by the red line in Fig. 14. (b)  
 4 Mean oxygen eddy flux normal to the section denoted by the blue line in Figure 14. (c) Horizontal  
 5 mean of (a) and (b) (red and blue lines, respectively). Gray contours denote oxygen concentrations, and  
 6 light red/blue contours correspond to positive/negative values of mean currents normal to the section  
 7 ( $1.0/-1.0 \text{ cm s}^{-1}$  in (a) and  $0.4/-0.2 \text{ cm s}^{-1}$  in (b)). White contour denotes the 0 value. The sign  
 8 convention was chosen so that a positive horizontal flux indicates transport towards the interior of the  
 9 OMZ.

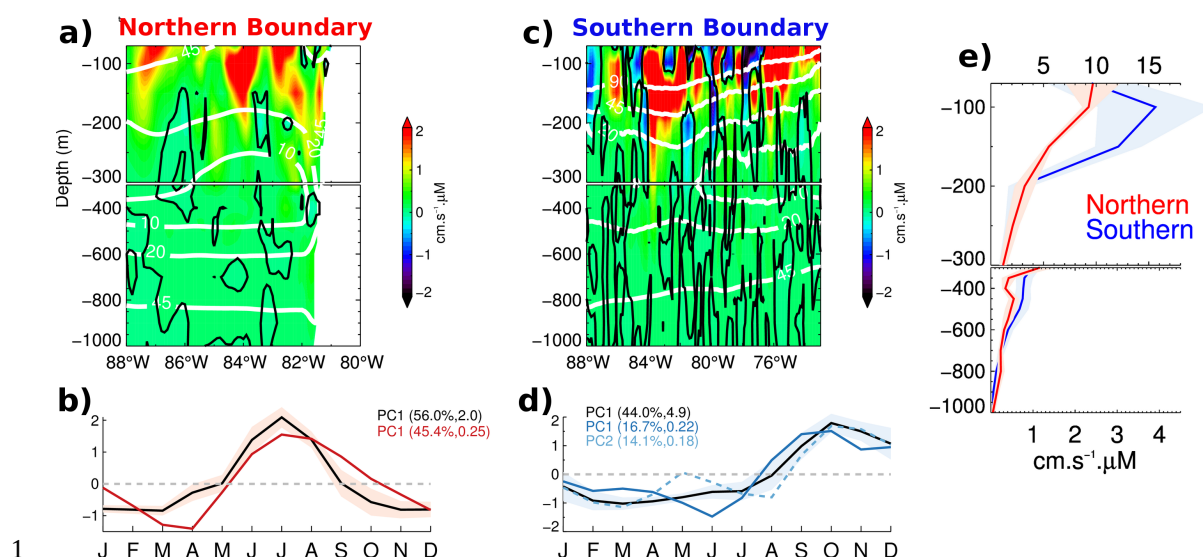
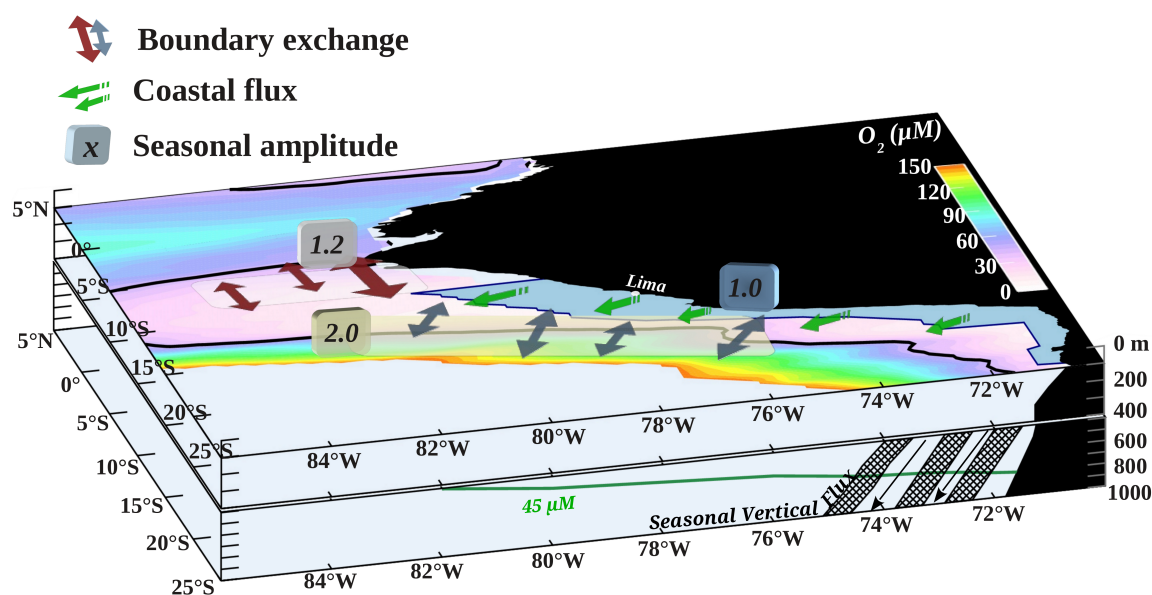


Figure 16. (a) Dominant EOF mode of the seasonal cycle of the oxygen eddy flux normal to the red section depicted in Figure 14. (b) Principal component associated to the EOF mode (black line). Red line corresponds to the seasonal cycle of the 30 days running variance of the (intraseasonal anomaly) currents (dominant EOF mode) normal to the section. (c) First EOF mode of the seasonal cycle of the oxygen eddy flux normal to the oblique section depicted in Fig. 14. (d) Principal component associated to the EOF pattern (black line) and seasonal cycle of the currents normal to the section (blue lines; computed as in (b)). Percentage of explained variance and RMS value are indicated in parenthesis (in  $\text{cm s}^{-1} \mu\text{M}$  and  $\text{cm s}^{-1}$ , for oxygen eddy flux and currents respectively). White contours in (a) and (c) denote mean oxygen concentration values, in  $\mu\text{M}$ . (e) RMS of the spatial patterns (a) and (c), computed along the horizontal direction. Note the scale leap at 300 m. Red/blue shading in (b), (d) and (e) represents a dispersion of  $\pm 1$  standard deviation, computed over a band  $2^\circ$  width around the sections depicted in Fig. 14.



1  
2

3 Figure 17. Schematic of the main processes driving the seasonal variability in the SEP OMZ: The  
 4 oxygen eddy flux through the northern-southern boundaries and the oxygen flux that extends from the  
 5 coastal boundary into the OMZ. The coastal band limits are defined by the light blue shading adjacent  
 6 to the coast. A scale of the seasonal amplitude of the eddy driven DO flux at each OMZ boundary is  
 7 indicated (units in  $\text{cm s}^{-1} \mu\text{M}$ ). The position of the  $45 \mu\text{M}$  is also represented (thick black contours).  
 8 The vertical/offshore oxygen flux induced by the propagation of the annual ETRW across the lower  
 9 oxycline is represented in the bottom panel.